

24

25 *Equal contribution

26

27 #Send correspondence to Saurabh Mehandru: saurabh.mehandru@mssm.edu, Paul D. Bieniasz:

28 pbieniasz@rockefeller.edu, Marina Caskey: mcaskey@rockefeller.edu, or Michel C.

29 Nussenzweig: nussen@rockefeller.edu

30

31 **SARS-CoV-2 has infected 47 million individuals and is responsible for over 1.2 million deaths**
32 **to date. Infection is associated with development of variable levels of antibodies with**
33 **neutralizing activity that can protect against infection in animal models. Antibody levels**
34 **decrease with time, but the nature and quality of the memory B cells that would be called**
35 **upon to produce antibodies upon re-infection has not been examined. Here we report on the**
36 **humoral memory response in a cohort of 87 individuals assessed at 1.3 and 6.2 months after**
37 **infection. We find that IgM, and IgG anti-SARS-CoV-2 spike protein receptor binding**
38 **domain (RBD) antibody titers decrease significantly with IgA being less affected.**
39 **Concurrently, neutralizing activity in plasma decreases by five-fold in pseudotype virus**
40 **assays. In contrast, the number of RBD-specific memory B cells is unchanged. Memory B**
41 **cells display clonal turnover after 6.2 months, and the antibodies they express have greater**
42 **somatic hypermutation, increased potency and resistance to RBD mutations, indicative of**
43 **continued evolution of the humoral response. Analysis of intestinal biopsies obtained from**
44 **asymptomatic individuals 3 months after COVID-19 onset, using immunofluorescence,**
45 **electron tomography or polymerase chain reaction, revealed persistence of SARS-CoV-2 in**
46 **the small bowel of 7 out of 14 volunteers. We conclude that the memory B cell response to**
47 **SARS-CoV-2 evolves between 1.3 and 6.2 months after infection in a manner that is**
48 **consistent with antigen persistence.**

49

50 Antibody responses to SARS-CoV-2 were initially characterized in a cohort of COVID-19-
51 convalescent individuals approximately 40 days (1.3 months) after infection ¹. Between 31 August
52 and 16 October 2020, 100 participants returned for a 6-month follow-up study visit. Although
53 initial criteria allowed enrollment of close contacts of individuals diagnosed with RT-PCR
54 confirmed SARS-CoV-2 infection ¹, 13 of the contacts did not seroconvert and were excluded
55 from further analyses. The remaining 87 participants with RT-PCR–confirmed COVID-19
56 diagnosis and/or seroconversion returned for analysis approximately 191 days (6.2 months, range:
57 165-223 days) after the onset of symptoms. In this cohort, symptoms lasted for a median of 12
58 days (0–44 days) during the acute phase, and 10 (11%) of the participants were hospitalized.
59 Consistent with other reports ^{2,3}, 38 (44%) of the participants reported persistent long-term
60 symptoms attributable to COVID-19 (Methods and Supplementary Tables 1 and 2). The duration
61 and severity of symptoms during acute disease was significantly greater among participants with
62 persistent post-acute symptoms at the second study visit (Extended Data Fig. 1m-o). Importantly,
63 all 87 participants tested negative for SARS-CoV-2 at the 6-month follow-up study visit using an
64 approved saliva-based PCR assay (Methods). Participant demographics and clinical characteristics
65 are shown in Supplementary Tables 1,2.

66
67 Antibody reactivity in plasma to RBD and nucleoprotein (N) was measured by validated
68 serological assays ^{1,4,5}. Two anti-RBD assays were strongly correlated (anti-RBD IgG and IgM
69 ELISA/Pylon-IgG and IgM at 1.3 months, $r=0.9200$ and $r=0.7543$, $p < 0.0001$, respectively.
70 Extended Data Fig 2). The IgM, IgG and IgA anti-RBD antibodies in plasma decreased
71 significantly between 1.3 and 6.2 months (Fig. 1a-c). However, the drop in RBD-binding activity
72 differed significantly by isotype, IgM showed the greatest decrease in anti-RBD reactivity (53%),

73 followed by IgG (33%) while IgA decreased by only 15% (Fig. 1e). In all cases the magnitude of
74 the decrease was inversely proportional to and directly correlated with the initial antibody levels
75 such that individuals with higher initial levels showed greater relative changes (Fig. 1f-i). In
76 contrast, the Roche anti-N assay⁵ showed a small but significant increase (19%) in reactivity
77 between the two time points that did not correlate with IgA anti-RBD ELISAs and was modestly
78 correlated with IgM at 1.3 months and IgG anti-RBD reactivity at both time points, respectively
79 (Fig. 1d and Extended Data Fig. 2i-n). Notably, individuals with persistent post-acute symptoms
80 had significantly higher anti-RBD IgG and anti-N antibody levels at both study visits (Extended
81 Data Fig. 1a-j).

82

83 Plasma neutralizing activity was measured using an HIV-1 virus pseudotyped with the SARS-
84 CoV-2 spike protein^{1,6}. Consistent with other reports the geometric mean half-maximal
85 neutralizing titer (NT₅₀) in this group of 87 participants was 401 and 78 at 1.3 and 6.2 months,
86 respectively, representing a five-fold decrease (Fig. 1j-k)^{7,8}. Neutralizing activity was directly
87 correlated with the IgG anti-RBD ELISA measurements (Extended data Fig. 2o-p). Moreover, the
88 absolute magnitude of the decrease in neutralizing activity was inversely proportional to and
89 directly correlated with the neutralizing activity at the earlier time point (Fig. 1l). We conclude
90 that antibodies to RBD and plasma neutralizing activity decrease significantly but remain
91 detectable 6 months after infection with SARS-CoV-2 in the majority of individuals.

92

93 Whereas plasma cells are the source of circulating antibodies, memory B cells contribute to recall
94 responses. To identify and enumerate the circulating SARS-CoV-2 memory B cell compartment
95 we used flow cytometry to isolate individual B lymphocytes with receptors that bound to RBD¹

96 (Fig. 2a and b, and Extended data Fig. 3). Notably, the percentage of RBD-binding memory B
97 cells increased marginally between 1.3 and 6.2 months in 21 randomly selected individuals (Fig.
98 2b).

99
100 To determine whether there were changes in the antibodies produced by memory B cells after 6.2
101 months, we obtained 532 paired antibody heavy and light chains from the same 6 individuals that
102 were examined at the earlier time point ¹ (Supplementary Table 3). There was no significant
103 difference in IGV gene representation at the two time points, including the over-representation of
104 the *IGHV3-30* and *3-53* gene segments ^{1,9-14} (Extended data Fig. 4). In keeping with this
105 observation, and similar to the earlier time point, antibodies that shared the same IGHV and IGLV
106 genes comprised 8.6% of all sequences in different individuals (Extended data Fig. 5a). As might
107 be expected, there was a small but significant overall increase in the percentage of IgG-expressing
108 anti-RBD memory cells, from 47% to 57% ($p=0.011$, Extended data Fig. 5b-d). Consistent with
109 the fractional increase in IgG memory cells, the extent of somatic hypermutation for both IGH and
110 IGL differed significantly in all 6 individuals between the two time points. Whereas the average
111 number of nucleotide mutations in IGH and IGL was only 4.2 and 2.8 at the first time point, these
112 values were increased to 11.7 and 6.5 at the second time point ($p<0.0001$, Fig. 2c and Extended
113 data Fig. 6). In contrast, the overall average IGH and IGL CDR3 length and hydrophobicity were
114 unchanged (Extended data Fig. 7).

115
116 Similar to the earlier time point, we found expanded clones of memory B cells at 6.2 months
117 including 23 that appeared at both time points. However, expanded clones accounted for only
118 12.4% of all antibody sequences after 6.2 months compared to 32% after 1.3 months ($p = 0.0225$,

119 Fig. 2d-e). In addition, the overall clonal composition of the memory compartment differed at the
120 two time points in all individuals examined (Fig. 2d). Forty-three expanded clones that were
121 present at the earlier time point were not detectable after 6.2 months while 22 new expanded clones
122 appeared. In addition, the relative distribution of clones that appeared at both time points also
123 varied. For example, the dominant clones in COV21 and COV57 representing 9.0% and 16.7% of
124 all sequences, respectively, were reduced to 1.1% and 1.9% of all sequences after 6.2 months (Fig.
125 2d and Supplementary Table 3). We conclude that while the magnitude of the RBD-specific
126 memory B cell compartment is conserved between 1.3 and 6.2 months after SARS-CoV-2
127 infection, there is significant clonal turnover and antibody sequence evolution, consistent with
128 prolonged germinal center reactions.

129
130 One hundred and twenty-two representative antibodies from the 6.2-month time point were tested
131 for reactivity to RBD (Supplementary Table 4). The antibodies that were evaluated included: (1)
132 49 that were randomly selected from those that appeared only once; (2) 23 that appeared as singles
133 at both 1.3 and 6.2 months; (3) 23 representatives of newly appearing expanded clones; (4) 27
134 representatives of expanded clones appearing at both time points. One hundred and fifteen of 122
135 of the antibodies bound to RBD indicating that flow cytometry efficiently identified B cells
136 producing anti-RBD antibodies (Fig. 3a and Supplementary Tables 4 and 5). Taking all antibodies
137 together, the mean ELISA EC_{50} was not significantly different at the two time points (Fig. 3a,
138 Supplementary Table 4 and ¹). However, comparison of the antibodies that were present at both
139 time points revealed a significant improvement of the EC_{50} after 6.2 months ($p= 0.0227$, Fig. 3b
140 and Extended data Fig.8a).

141

142 To determine whether the antibodies expressed by memory B cells at the late time point also
143 showed altered breadth, we compared them to earlier clonal relatives in binding assays using
144 control and mutant RBDs: The mutations E484K and Q493R¹⁵ were selected for resistance to class
145 2 antibodies such as C144 and C121 that bind directly to the ACE2 interaction ridge in the RBD
146 ^{1,16-18} while R346S, N439K, and N440K were selected for resistance to class 3 antibodies such as
147 C135 that do not directly interfere with ACE2 binding ^{1,15-18} (Fig.3c). In addition, V367F, A475V,
148 S477N, and V483A represent circulating variants that confer complete or partial resistance to class
149 1 and 2 antibodies ^{15,16,19} (Fig. 3c). Out of 52 antibody clonal pairs appearing at both time points,
150 43 (83%) showed overall increased binding to mutant RBDs at the 6.2-month time point (Extended
151 data Fig. 8b-k, Supplementary Table 5). For example, C144, an antibody recovered at the 1.3-
152 month time point, was unable to bind to Q493R or E484K RBDs, but all 4 of its 6.2-month clonal
153 derivatives bound to Q493R, and one also showed binding to E484K (Fig. 3d). Overall, the most
154 pronounced increase in binding occurred for RBD mutations in amino acid positions such as E484,
155 Q493, N439, N440 and R346 that are critical for binding of class 2 and 3 antibodies ^{15,16} (Fig. 3e,
156 Extended data Fig. 8b-k and Supplementary Table 5).

157

158 Next, all 122 antibodies from the 6.2 month time point were tested for activity in a pseudotyped
159 SARS-CoV-2 neutralization assay ^{1,6} (Fig. 4a, Supplementary Table 6). Consistent with RBD
160 binding assays, the mean neutralization IC₅₀ values were not significantly different at the two time
161 points when all antibodies were compared (Fig. 4a and ¹). However, comparison of the antibodies
162 that were present at both time points revealed a significant improvement of the IC₅₀ values at 6.2
163 months (p=0.0003, Fig. 4b and Extended data Fig. 9a).

164

165 To determine whether the antibodies exhibiting altered RBD binding also show increased
166 neutralizing breadth, we tested 5 representative antibody pairs recovered at the two time points
167 against HIV-1 viruses pseudotyped with E484G, Q493R, and R346S mutant spike proteins (Fig.
168 4c, Supplementary Table 6). Notably, the Q493R and E484G pseudotyped viruses were resistant
169 to neutralization by C144; in contrast, its 6.2-month clonal derivative C051 neutralized both
170 variants with IC_{50} values of 4.7 and 3.1 ng/ml respectively (Fig. 4c-d). Similarly, R346S
171 pseudotyped viruses were resistant to C032, but a 6.2-month clonal derivative C080 neutralized
172 this variant with an IC_{50} of 5.3 ng/ml (Fig. 4c, Extended data Fig. 9b-f). Consistent with the
173 observed changes in binding and neutralizing activity several late-appearing antibodies (e.g. C051)
174 had acquired mutations directly in or adjacent to the RBD-binding paratope (Fig. 4e, Extended
175 data Fig. 10). We conclude that memory B cells that evolved during the observation period express
176 antibodies with increased neutralizing potency and breadth.

177
178 Antibody evolution occurs by somatic mutation and selection in germinal centers wherein antigen
179 can be retained in the form of immune complexes on the surface of follicular dendritic cells for
180 prolonged periods of time. Residual virus in tissues represents another potential source of antigen.
181 SARS-CoV-2 replicates in ACE2-expressing cells in the lungs, nasopharynx and small intestine
182 ²⁰⁻²³, and viral RNA has been detected in stool samples even after the virus is cleared from the
183 nasopharynx ²⁴⁻²⁶. To determine whether there might be antigen persistence in the intestine after
184 resolution of clinical illness, we obtained biopsies from the upper and lower gastrointestinal (GI)
185 tract of 14 individuals, an average of 4 months (range 2.8-5.5 months) after initial SARS-CoV-2
186 diagnosis (Supplementary Table 7). Clinically approved nasopharyngeal swab PCR assays were
187 negative in all 14 individuals at the time of biopsy. However, biopsy samples from 3 of the 14

188 participants produced PCR amplicons that were sequence verified as SARS-CoV-2 (Methods and
189 Supplementary Table 7). Immunostaining was performed to determine whether viral protein was
190 also detectable in upper and lower GI tract, with de-identified biopsies from individuals pre-dating
191 the pandemic (n=10) serving as controls. ACE2 and SARS-CoV-2 N protein was detected in
192 intestinal enterocytes in 5 of 14 individuals but not in historic control samples (Fig. 5a-d, Extended
193 data Fig. 11,12 and 13, and Supplementary Table 7). When detected, immunostaining was
194 sporadic, patchy, exclusive to the intestinal epithelium and not associated with inflammatory
195 infiltrates (Extended data Fig. 11,12).

196
197 Detection of SARS-CoV-2 RNA and N protein could represent defective viral particles and/or
198 infected cell debris. To determine whether viral particles were present we used electron
199 tomography to examine a tissue sample from one of the individuals who was positive by
200 immunofluorescence (Fig. 5e-j). Particles with typical SARS-CoV-2 morphologies were found
201 within intracellular membrane-enclosed vesicles consistent with coronavirus exit compartments in
202 terminal ileum apical epithelial cells (Fig. 5e-h), suggesting the presence of intact virions. Particles
203 were also found in vesicles in apical epithelial cells of the duodenum, although there were fewer
204 and less densely-populated vesicles observed (Fig. 5i-j).

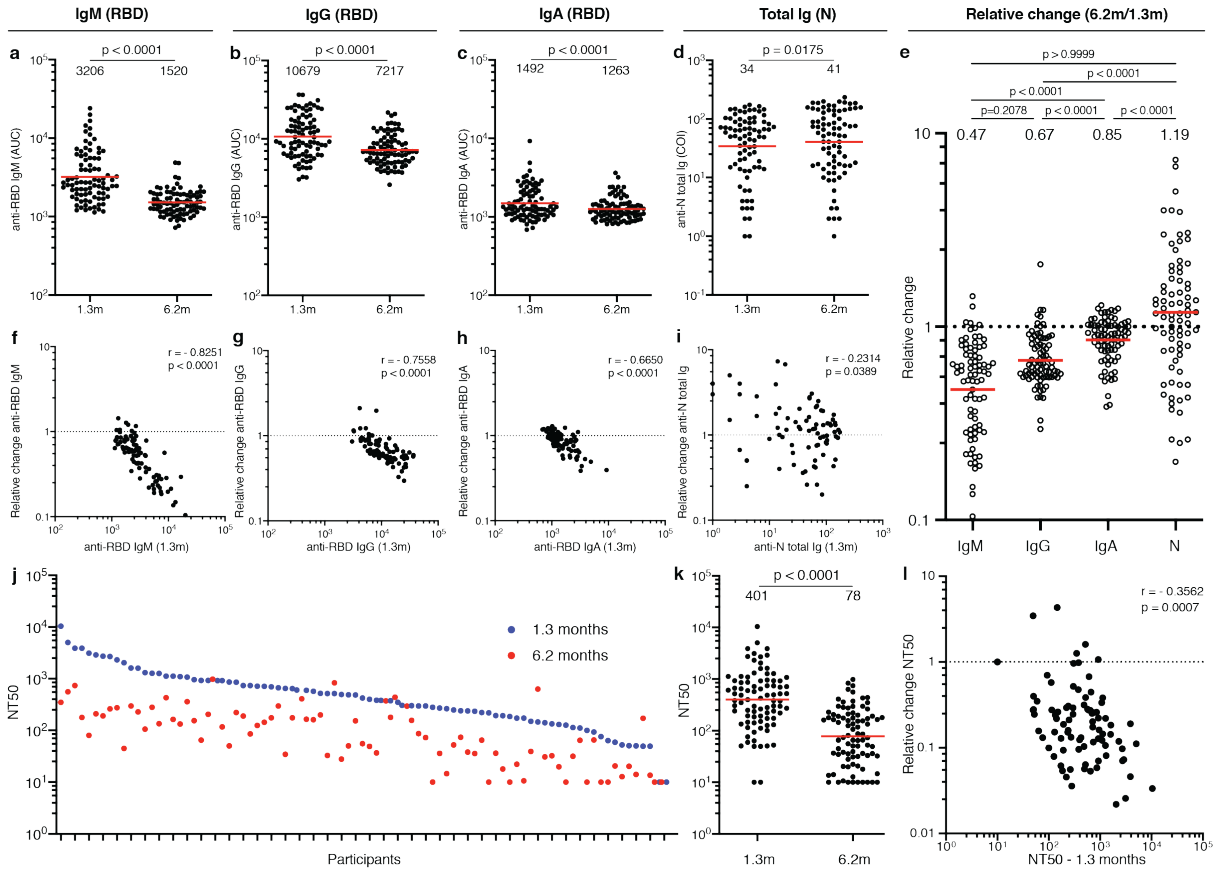
205
206 Neutralizing antibodies to SARS-CoV-2 develop in most individuals after infection but decay with
207 time ^{7,8,27-31}. These antibodies are effective in prevention and therapy in animal models and are
208 likely to play a role in protection from re-infection in humans ³². Although there is a significant
209 drop in plasma neutralizing activity between 1.3 and 6.2 months, antibody titers remain measurable
210 in most individuals ^{7,8,27-30,33}.

211
212 Neutralizing monoclonal antibodies obtained from individuals during the early convalescence
213 period showed remarkably low levels of somatic mutations that some investigators attributed to
214 defects in germinal center formation ^{9,10,12,34-37}. Our data indicate that the anti-SARS-CoV-2
215 memory B cell response evolves during the first 6 months after infection, with accumulation of Ig
216 somatic mutations, and production of antibodies with increased neutralizing breadth and potency.
217 Persistent antibody evolution occurs in germinal centers and requires that B cells are exposed to
218 antigen trapped in the form of immune complexes on follicular dendritic cells ³⁸. This form of
219 antigen can be long-lived because follicular dendritic cells do not internalize immune complexes.
220 In addition, even small amounts of persistent viral replication could contribute antigen to fuel
221 antibody evolution. The observation that SARS-CoV-2 remains detectable in the small intestinal
222 epithelium even 3 months after infection is consistent with the relative persistence of anti-RBD
223 IgA antibodies and continued antibody evolution. However, the prevalence, clinical significance,
224 and potential infectivity of residual SARS-CoV-2 in intestinal enterocytes remain to be
225 determined.

226
227 Memory responses are responsible for protection from re-infection and are essential for effective
228 vaccination. The observation that memory B cell responses do not decay after 6.2 months, but
229 instead continue to evolve, is strongly suggestive that individuals who are infected with SARS-
230 CoV-2 could mount a rapid and effective response to the virus upon re-exposure.

231

232 **Figures**



233

234

235 **Fig. 1: Plasma antibody dynamics against SARS-CoV-2.**

236 **a–d**, Results of serological assays measuring plasma reactivity to RBD (**a,b,c**) and N protein (**d**)

237 at the initial 1.3 and 6.2 month follow-up visit, respectively. **a**, Anti-RBD IgM. **b**, Anti-RBD IgG.

238 **c**, Anti-RBD IgA **d**, Anti-N total antibodies. The normalized area under the curve (AUC) values

239 for 87 individuals and Cut-off Index (COI) values for 80 individuals are shown in **a,b,c** and **d** for

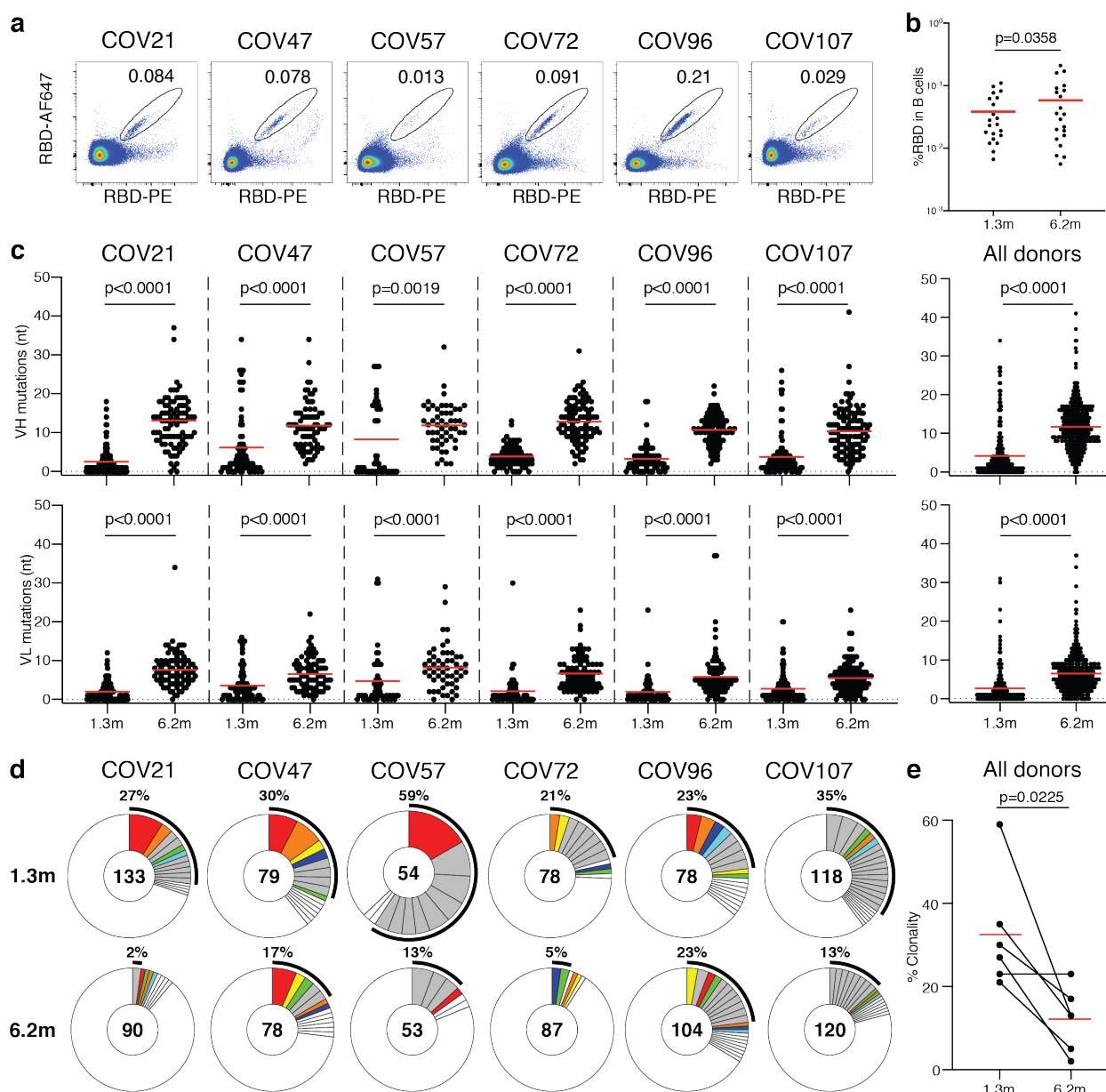
240 both time points, respectively. Positive and negative controls were included for validation ¹. **e**,

241 Relative change in plasma antibody levels between 1.3 and 6.2 months for anti-RBD IgM, IgG,

242 IgA and anti-N total Ig, respectively. **f-i**, Relative change in antibody levels between 1.3 and 6.2

243 months plotted against the corresponding antibody levels at 1.3 months. **f**, Anti-RBD IgM. $r = -$
244 0.83 , $p < 0.0001$. **g**, Anti-RBD IgG. $r = -0.76$, $p < 0.0001$. **h**, Anti-RBD IgA. $r = -0.67$, $p < 0.0001$.
245 **i**, Anti-N total antibodies. $r = -0.23$, $p = 0.039$. **j**. Ranked average half-maximal inhibitory plasma
246 neutralizing titer (NT50) at 1.3 months (blue) and 6.2 months (red) for the 87 individuals studied.
247 **k**. Graph shows NT50 for plasma collected at 1.3 and 6.2 months $p < 0.0001$. **l**. Relative change in
248 plasma neutralizing titers between 1.3 and 6.2 months plotted against the corresponding titers at
249 1.3 months. For **a-e**, **k** plotted values and horizontal bars indicate geometric mean. Statistical
250 significance was determined using Wilcoxon matched-pairs signed rank test in **a-d**, **k** and
251 Friedman with Dunn's multiple comparison test in **e**. The r and p values in **f – l** and **l** were
252 determined by two-tailed Spearman's correlations.

253

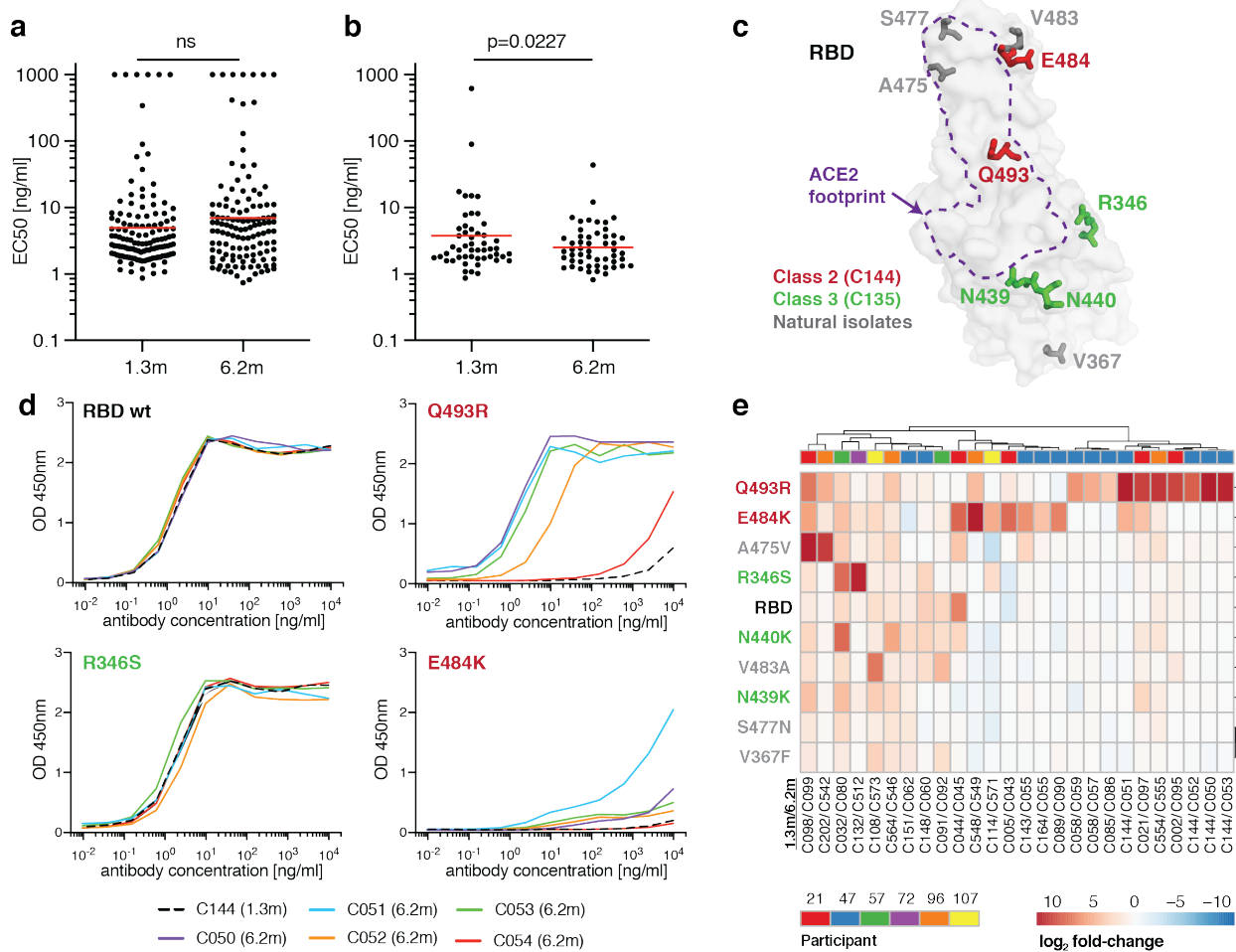


254

255 **Fig. 2: Anti-SARS-CoV-2 RBD antibody sequences.**

256 **a**, Representative flow cytometry plots showing dual AlexaFluor-647–RBD- and PE–RBD-
 257 binding B cells for six study individuals (gating strategy is in Extended Data Fig.3). Percentage of
 258 antigen-specific B cells is indicated. **b**. As in **a**. graph summarizes %RBD binding memory B cells
 259 in samples obtained at 1.3 and 6.2 months from 21 randomly selected individuals. Red horizontal
 260 bars indicate geometric mean values. Statistical significance was determined using Wilcoxon

261 matched-pairs signed rank test. **c**, Number of somatic nucleotide mutations in the IGVH (top) and
262 IGVL (bottom) in antibodies obtained after 1.3 or 6.2 months from the indicated individual or all
263 donors (right). **d**, Pie charts show the distribution of antibody sequences from 6 individuals after
264 1.3¹ (upper panel) or 6.2 months (lower panel). The number in the inner circle indicates the number
265 of sequences analyzed for the individual denoted above the circle. Pie slice size is proportional to
266 the number of clonally related sequences. The black outline indicates the frequency of clonally
267 expanded sequences detected in each patient. Colored slices indicate persisting clones (same IGHV
268 and IGLV genes and highly similar CDR3s) found at both timepoints in the same patient. Grey
269 slices indicate clones unique to the timepoint. White slices indicate singlets found at both
270 timepoints, while the remaining white area indicates sequences isolated once. **e**. Graph shows
271 relative clonality at both time points timepoints. Red horizontal bars indicate mean values.
272 Statistical significance was determined using two-tailed Mann–Whitney U-tests or paired t-test.

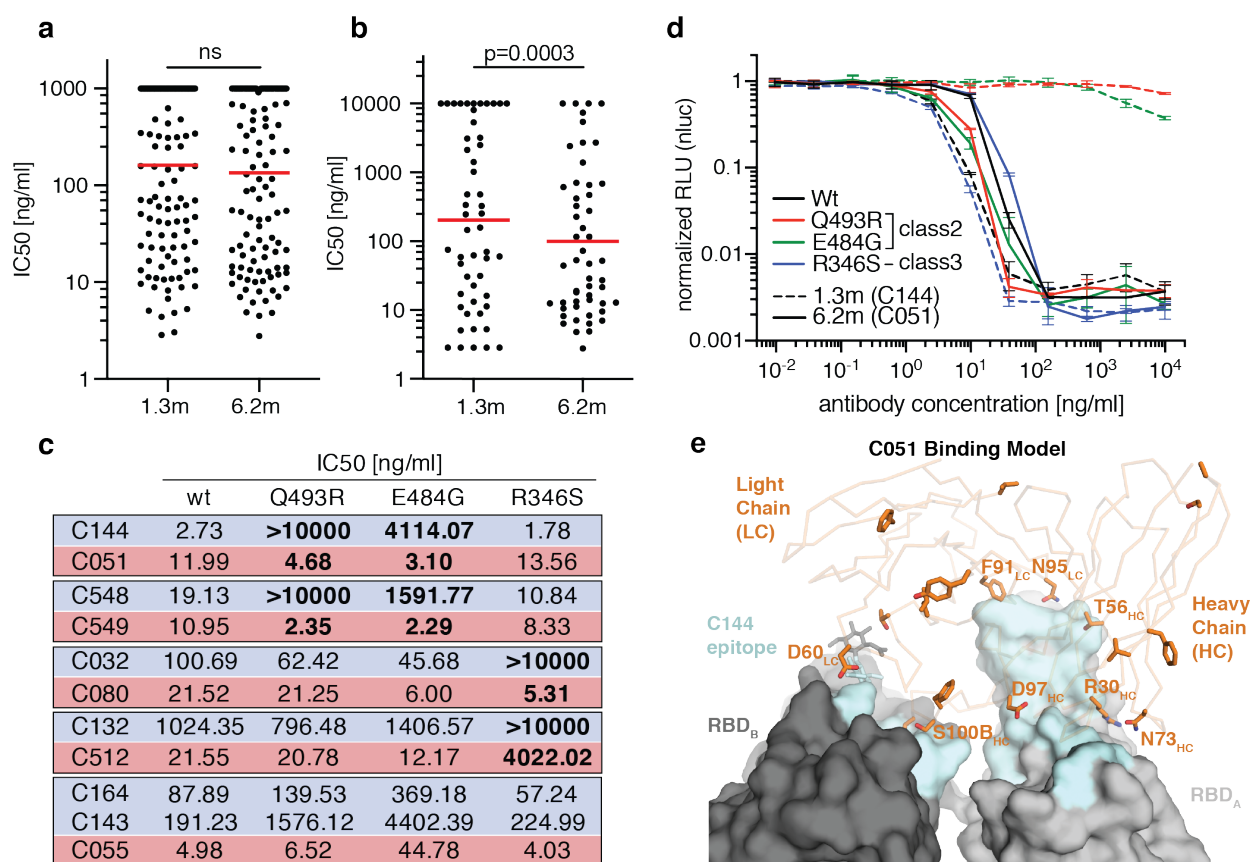


273

274 **Fig. 3: Anti-SARS-CoV-2 RBD monoclonal antibody reactivity.**

275 **a**, Graphs show anti-SARS-CoV-2 RBD antibody reactivity. ELISA EC₅₀ values for all antibodies
 276 measured at 1.3¹ and 122 selected monoclonal antibodies at 6.2 months. Horizontal bars indicate
 277 geometric mean. Statistical significance was determined using Mann–Whitney U-test. **b**, EC₅₀
 278 values for all antibodies that appear at 1.3 and 6.2 months. Average of two or more experiments.
 279 Horizontal bars indicate geometric mean. Statistical significance was determined using Wilcoxon
 280 matched-pairs signed rank test. **c**, Surface representation of the RBD with the ACE2 binding
 281 footprint indicated as a dotted line and selected residues found in circulating strains (grey) and
 282 residues that mediate resistance to class 2 (red, C144) and 3 (green, C135) antibodies highlighted

283 as sticks. **d.** Graphs show ELISA binding curves for C144 (black dashed line) and its clonal
 284 relatives obtained after 6.2 months (C050-54, solid lines) binding to wild type, Q493R, R346S,
 285 and E484K mutant RBDs. **e.** Heat map shows log₂ relative fold change in EC₅₀ against indicated
 286 RBD mutants for 26 antibody clonal pairs obtained at 1.3 and 6.2 month with the most pronounced
 287 changes in reactivity. The participant origin for each antibody pair is indicated above. All
 288 experiments were performed at least twice.



289

290 **Fig.4: Anti-SARS-CoV-2 RBD monoclonal antibody neutralizing activity.**

291 **a,** SARS-CoV-2 pseudovirus neutralization assay. IC₅₀ values for all antibodies measured at 1.3
 292 months¹ and 122 selected antibodies at 6.2 months. Antibodies with IC₅₀ values above 1 μg/ml
 293 were plotted at 1 μg/ml. Mean of 2 independent experiments. Red bar indicates geometric mean.

294 Statistical significance was determined using Mann-Whitney U-test. **b**, IC₅₀ values for antibodies
295 appearing at 1.3 and 6.2 months. Red bar indicates geometric mean. Statistical significance was
296 determined using Wilcoxon matched-pairs signed rank test. **c**, IC₅₀ values for 5 different pairs of
297 mAb clonal relatives obtained after 1.3 (blue) or 6.2 months (red) for neutralization of wild type
298 and mutant SARS-CoV-2 pseudovirus. Antibody IDs of the 1.3 months/6.2 months mAb pairs as
299 indicated. **d**, Graph shows the normalized relative luminescence values for cell lysates of 293T_{ACE2}
300 cells 48 hpi with SARS-CoV-2 pseudovirus harboring wt RBD or mutant RBDs (wt, Q493R,
301 E484G, R346S RBD mutants are shown in black, red, green and blue, respectively) in the presence
302 of increasing concentrations of mAbs C144 (1.3 months, dashed lines) or C051 (6.2 months, solid
303 lines). **e**, Surface representation of two adjacent “down” RBDs (RBD_A and RBD_B) on a spike
304 trimer with the C144 epitope on the RBDs highlighted in cyan and positions of amino acid
305 mutations that accumulated in C051 compared to the parent antibody C144 highlighted as stick
306 side chains on a C α atom representation C051 V_HV_L binding to adjacent RBDs. The C051
307 interaction with two RBDs was modeled based on a cryo-EM structure of C144 Fab bound to spike
308 trimer¹⁶.

310 **Fig. 5: Immunofluorescence and electron microscopy imaging of intestinal biopsies.**

311 **a**, Immunofluorescence images of human enterocytes stained for EPCAM (red), DAPI (blue) and
312 either ACE2 (green, **a** and **c**) or SARS-CoV-2 N (green, **b** and **d**) in intestinal biopsies taken 92
313 days after COVID-19 symptom onset of participant CGI-088 in the terminal ileum (**a-b**) or
314 duodenum (**c-d**). Arrows indicate enterocytes with detectable SARS-CoV-2 antigen. White scale
315 bar corresponds to 100 μ m. **e-h**, SARS-CoV-2 virions within terminal ileum of CGI-088
316 (identified as described in methods). **e**, Montaged 2D overview of a region of apical epithelium.
317 **f**, Tomographic slice (1.5 nm) of a 3D reconstruction of the area of epithelial cell cytoplasm
318 indicated by the white square in **e**. Two coronavirus-filled exit compartments (center) are
319 surrounded by other membranous compartments with dissimilar contents. **g**, Tomographic detail
320 of the two exit compartments, indicated by the white rectangle in **f**. Each compartment contains
321 ~20 presumptive SARS-CoV-2 virions. **h**, Detail of a single virion (indicated by white arrow in **g**)
322 showing densities for the membrane bilayer (black arrowhead), punctate core structures (*), and
323 surface spikes (red dots). **i-j**, SARS-CoV-2 within duodenum of CGI-088 (identified as described
324 in methods). **i**, Montaged 2D overview of a region of the duodenal apical epithelium. **j**,
325 Tomographic slice (1.5 nm) of a 3D reconstruction of the area of epithelial cell cytoplasm indicated
326 by the white square in **i**. SARS-CoV-2 virions are localized to two smooth-walled exit
327 compartments (white arrows). Inset in **j**: Detail of three presumptive SARS-CoV-2 virions from
328 the compartment in the upper left of **j**. Surface spikes are indicated by red dots. M, Mitochondrion.
329

330 **Methods**

331

332 **Data reporting**

333 No statistical methods were used to predetermine sample size. The experiments were not
334 randomized and the investigators were not blinded to allocation during experiments and outcome
335 assessment.

336

337 **Study participants.** Previously enrolled study participants ¹ were asked to return for a 6-month
338 follow-up visit at the Rockefeller University Hospital in New York from August 31 through
339 October 16, 2020. Eligible participants were adults aged 18-76 years and were either diagnosed
340 with SARS-CoV-2 infection by RT-PCR (cases), or were close contacts (e.g., household, co-
341 workers, members of same religious community) with someone who had been diagnosed with
342 SARS-CoV-2 infection by RT-PCR (contacts). Close contacts without seroconversion against
343 SARS-CoV-2 as assessed by serological assays (described below) were not included in the
344 subsequent analysis. Most study participants were residents of the Greater New York City tri-state
345 region and were asked to return approximately 6 months after the time of onset of COVID-19
346 symptoms. Participants presented to the Rockefeller University Hospital for blood sample
347 collection and were asked to recall the symptoms and severity of clinical presentation during the
348 acute (first 6 weeks) and the convalescent (7 weeks until second study visit) phase of COVID-19,
349 respectively. The severity of acute infection was assessed by the WHO Ordinal Clinical
350 Progression/Improvement Scale ([https://www.who.int/publications/i/item/covid-19-therapeutic-](https://www.who.int/publications/i/item/covid-19-therapeutic-trial-synopsis)
351 [trial-synopsis](https://www.who.int/publications/i/item/covid-19-therapeutic-trial-synopsis)). Shortness of breath was assessed through the modified Medical Research Council
352 (mMRC) dyspnea scale ³⁹. Participants who presented with persistent symptoms attributable to
353 COVID-19 were identified on the basis of chronic shortness of breath or fatigue, deficit in athletic

354 ability and/or three or more additional long-term symptoms such as persistent unexplained fevers,
355 chest pain, new-onset cardiac sequelae, arthralgias, impairment of concentration/mental acuity,
356 impairment of sense of smell/taste, neuropathy or cutaneous findings ^{2,3}. All participants at
357 Rockefeller University provided written informed consent before participation in the study and the
358 study was conducted in accordance with Good Clinical Practice.

359
360 **Gastrointestinal biopsy cohort.** To determine if SARS-CoV-2 can persist in the gastrointestinal
361 tract, we recruited a cohort of 14 individuals with prior diagnosis of and recovery from COVID-
362 19 illness. Eligible participants included adults, 18-76 years of age who were previously diagnosed
363 with SARS-CoV-2 by RT PCR and presented to the gastroenterology clinics of Mount Sinai
364 Hospital. Endoscopic procedures were performed for clinically indicated conditions as detailed in
365 Supplementary Table 7. All participants were asymptomatic at the time of the endoscopic
366 procedures and negative for SARS-CoV-2 by nasal swab PCR (Cycle threshold (Ct) cut-off <38⁴⁰).
367 Informed consent was obtained from all participants. The biopsy-related studies were approved by
368 the Mount Sinai Ethics Committee/IRB (IRB 16-0583, The impact of viral infections and their
369 treatment on gastrointestinal immune cells).

370
371 **SARS-CoV-2 saliva PCR test**
372 Saliva was collected into guanidine thiocyanate buffer as described ⁴¹. RNA was extracted using
373 either a column-based (Qiagen QIAmp DSP Viral RNA Mini Kit, Cat#61904) or a magnetic bead-
374 based method as described ⁴². Reverse transcribed cDNA was amplified using primers and probes
375 validated by the CDC or by Columbia University Personalized Medicine Genomics Laboratory,

376 respectively, and approved by the FDA under the Emergency Use Authorization. Viral RNA was
377 considered detected if the cycle threshold (Ct) for two viral primers/probes were <40.

378

379 **Blood samples processing and storage.** Peripheral Blood Mononuclear Cells (PBMCs) were
380 obtained by gradient centrifugation and stored in liquid nitrogen in the presence of FCS and
381 DMSO. Heparinized plasma and serum samples were aliquoted and stored at -20°C or less. Prior
382 to experiments, aliquots of plasma samples were heat-inactivated (56°C for 1 hour) and then stored
383 at 4°C.

384

385 **High throughput automated serology assays**

386 Plasma samples from 80 out of 87 participants were tested by high throughput automated serology
387 assays. The Roche Elecsys anti-SARS-CoV-2 assay was performed on Roche Cobas e411 (Roche
388 Diagnostics, Indianapolis, IN). The Elecsys anti-SARS-CoV-2 assay uses a recombinant protein
389 representing the N antigen for the determination of antibodies against SARS-CoV-2. This assay
390 received Emergency Use Authorization (EUA) approval from the United States Food and Drug
391 Administration (FDA) ⁵. The Pylon COVID-19 IgG and IgM assays were used to measure plasma
392 IgG and IgM antibodies against SARS-CoV-2, respectively. Plasma samples were assayed on the
393 Pylon 3D analyzer (ET HealthCare, Palo Alto, CA) as previously described ⁴. This assay was
394 implemented clinically as a laboratory-developed test under New York State Department of Health
395 regulations. Briefly, the assay was performed using a unitized test strip containing wells with pre-
396 dispensed reagents. The COVID-19 reagent contains biotinylated recombinant versions of the
397 SARS-CoV-2 S-Protein RBD and trace amounts of N protein as antigens that bind IgG and IgM,
398 respectively. The cut off values for both Pylon assays were determined using the mean of non-

399 COVID-19 samples plus 6 Standard Deviations (SDs). The results of a sample are reported in the
400 form of a cutoff index (COI) or an index value (IV), which were determined by the instrument
401 readout of the test sample divided by instrument readout at cut off.

402

403 **ELISAs**

404 Validated ELISAs^{43,44} to evaluate antibodies binding to SARS-CoV-2 RBD and additional RBDs
405 were performed by coating of high-binding 96-half-well plates (Corning 3690) with 50 µl per well
406 of a 1 µg/ml protein solution in PBS overnight at 4 °C. Plates were washed 6 times with washing
407 buffer (1× PBS with 0.05% Tween-20 (Sigma-Aldrich)) and incubated with 170 µl per well
408 blocking buffer (1× PBS with 2% BSA and 0.05% Tween-20 (Sigma)) for 1 h at room temperature.
409 Immediately after blocking, monoclonal antibodies or plasma samples were added in PBS and
410 incubated for 1 h at room temperature. Plasma samples were assayed at a 1:67 starting dilution and
411 7 additional threefold serial dilutions. Monoclonal antibodies were tested at 10 µg/ml starting
412 concentration and 10 additional fourfold serial dilutions. Plates were washed 6 times with washing
413 buffer and then incubated with anti-human IgG, IgM or IgA secondary antibody conjugated to
414 horseradish peroxidase (HRP) (Jackson Immuno Research 109-036-088 109-035-129 and Sigma
415 A0295) in blocking buffer at a 1:5,000 dilution (IgM and IgG) or 1:3,000 dilution (IgA). Plates
416 were developed by addition of the HRP substrate, TMB (ThermoFisher) for 10 min (plasma
417 samples) or 4 minutes (monoclonal antibodies), then the developing reaction was stopped by
418 adding 50 µl 1 M H₂SO₄ and absorbance was measured at 450 nm with an ELISA microplate
419 reader (FluoStar Omega, BMG Labtech) with Omega and Omega MARS software for analysis.
420 For plasma samples, a positive control (plasma from patient COV72, diluted 66.6-fold and seven
421 additional threefold serial dilutions in PBS) was added to every assay plate for validation. The

422 average of its signal was used for normalization of all of the other values on the same plate with
423 Excel software before calculating the area under the curve using Prism V8.4 (GraphPad). For
424 monoclonal antibodies, the EC50 was determined using four-parameter nonlinear regression
425 (GraphPad Prism V8.4).

426

427 **Expression of RBD proteins**

428 Mammalian expression vectors encoding the RBDs of SARS-CoV-2 (GenBank MN985325.1; S
429 protein residues 319-539) and eight additional mutant RBD proteins (E484K, Q493R, R346S,
430 N493K, N440K, V367F, A475V, S477N and V483A) with an N-terminal human IL-2 or Mu
431 phosphatase signal peptide were previously described ⁴⁵.

432

433 **SARS-CoV-2 pseudotyped reporter virus**

434 SARS-CoV-2 pseudotyped particles were generated as previously described ^{1,46}. Briefly, 293T
435 cells were transfected with pNL4-3ΔEnv-nanoluc and pSARS-CoV-2-S_{Δ19}. For generation of
436 RBD-mutant pseudoviruses, pSARS-CoV-2-S_{Δ19} carrying either of the following spike mutations
437 was used instead of its wt counterpart: Q493R, R346S or E484G ⁴⁷. Particles were harvested 48
438 hpt, filtered and stored at -80°C.

439

440 **Pseudotyped virus neutralization assay**

441 Fourfold serially diluted plasma from COVID-19-convalescent individuals or monoclonal
442 antibodies were incubated with SARS-CoV-2 pseudotyped virus for 1 h at 37 °C. The mixture was
443 subsequently incubated with 293T_{Acc2} cells for 48 h after which cells were washed with PBS and
444 lysed with Luciferase Cell Culture Lysis 5× reagent (Promega). Nanoluc Luciferase activity in

445 lysates was measured using the Nano-Glo Luciferase Assay System (Promega) with the Glomax
446 Navigator (Promega). The obtained relative luminescence units were normalized to those derived
447 from cells infected with SARS-CoV-2 pseudotyped virus in the absence of plasma or monoclonal
448 antibodies. The half-maximal inhibitory concentration for plasma (NT₅₀) or monoclonal antibodies
449 (IC₅₀) was determined using four-parameter nonlinear regression (least squares regression method
450 without weighting; constraints: top=1, bottom=0) (GraphPad Prism).

451

452 **Biotinylation of viral protein for use in flow cytometry**

453 Purified and Avi-tagged SARS-CoV-2 RBD was biotinylated using the Biotin-Protein Ligase-
454 BIRA kit according to manufacturer's instructions (Avidity) as described before ¹. Ovalbumin
455 (Sigma, A5503-1G) was biotinylated using the EZ-Link Sulfo-NHS-LC-Biotinylation kit
456 according to the manufacturer's instructions (Thermo Scientific). Biotinylated ovalbumin was
457 conjugated to streptavidin-BV711 (BD biosciences, 563262) and RBD to streptavidin-PE (BD
458 Biosciences, 554061) and streptavidin-AF647 (Biolegend, 405237)¹.

459

460 **Single-cell sorting by flow cytometry**

461 Single-cell sorting by flow cytometry was described previously ¹. Briefly, peripheral blood
462 mononuclear cells were enriched for B cells by negative selection using a pan-B-cell isolation kit
463 according to the manufacturer's instructions (Miltenyi Biotec, 130-101-638). The enriched B cells
464 were incubated in FACS buffer (1× PBS, 2% FCS, 1 mM EDTA) with the following anti-human
465 antibodies (all at 1:200 dilution): anti-CD20-PECy7 (BD Biosciences, 335793), anti-CD3-APC-
466 eFluro 780 (Invitrogen, 47-0037-41), anti-CD8-APC-eFluor 780 (Invitrogen, 47-0086-42), anti-
467 CD16-APC-eFluor 780 (Invitrogen, 47-0168-41), anti-CD14-APC-eFluor 780 (Invitrogen, 47-

468 0149-42), as well as Zombie NIR (BioLegend, 423105) and fluorophore-labelled RBD and
469 ovalbumin (Ova) for 30 min on ice. Single CD3⁻CD8⁻CD14⁻CD16⁻CD20⁺Ova⁻RBD-
470 PE⁺RBD-AF647⁺ B cells were sorted into individual wells of 96-well plates containing 4 µl of
471 lysis buffer (0.5× PBS, 10 mM DTT, 3,000 units/ml RNasin Ribonuclease Inhibitors (Promega,
472 N2615) per well using a FACS Aria III and FACSDiva software (Becton Dickinson) for
473 acquisition and FlowJo for analysis. The sorted cells were frozen on dry ice, and then stored at
474 -80 °C or immediately used for subsequent RNA reverse transcription.

475

476 **Antibody sequencing, cloning and expression**

477 Antibodies were identified and sequenced as described previously ¹. In brief, RNA from single
478 cells was reverse-transcribed (SuperScript III Reverse Transcriptase, Invitrogen, 18080-044) and
479 the cDNA stored at -20 °C or used for subsequent amplification of the variable IGH, IGL and IGK
480 genes by nested PCR and Sanger sequencing. Sequence analysis was performed using MacVector.
481 Amplicons from the first PCR reaction were used as templates for sequence- and ligation-
482 independent cloning into antibody expression vectors. Recombinant monoclonal antibodies and
483 Fabs were produced and purified as previously described ¹.

484

485 **Computational analyses of antibody sequences**

486 Antibody sequences were trimmed based on quality and annotated using Igblastn v.1.14. with
487 IMGT domain delineation system. Annotation was performed systematically using Change-O
488 toolkit v.0.4.540 ⁴⁸. Heavy and light chains derived from the same cell were paired, and clonotypes
489 were assigned based on their V and J genes using in-house R and Perl scripts (Extended data Fig.4).

490 All scripts and the data used to process antibody sequences are publicly available on GitHub
491 (<https://github.com/stratust/igpipeline>).

492

493 The frequency distributions of human V genes in anti-SARS-CoV-2 antibodies from this study
494 was compared to 131,284,220 IgH and IgL sequences generated by ⁴⁹ and downloaded from cAb-
495 Rep⁵⁰, a database of human shared BCR clonotypes available at [https://cab-](https://cab-rep.c2b2.columbia.edu/)
496 [rep.c2b2.columbia.edu/](https://cab-rep.c2b2.columbia.edu/). Based on the 82 distinct V genes that make up the 1703 analyzed
497 sequences from Ig repertoire of the three patients present in this study, we selected the IgH and
498 IgL sequences from the database that are partially coded by the same V genes and counted them
499 according to the constant region. The frequencies shown in (Fig. S4) are relative to the source and
500 isotype analyzed. We used the two-sided binomial test to check whether the number of sequences
501 belonging to a specific IgHV or IgLV gene in the repertoire is different according to the frequency
502 of the same IgV gene in the database. Adjusted p-values were calculated using the false discovery
503 rate (FDR) correction. Significant differences are denoted with stars.

504

505 Nucleotide somatic hypermutation and CDR3 length were determined using in-house R and Perl
506 scripts. For somatic hypermutations, IGHV and IGLV nucleotide sequences were aligned against
507 their closest germlines using Igbblastn and the number of differences were considered nucleotide
508 mutations. The average mutations for V genes was calculated by dividing the sum of all nucleotide
509 mutations across all patients by the number of sequences used for the analysis. To calculate the
510 GRAVY scores of hydrophobicity ⁵¹ we used Guy H.R. Hydrophobicity scale based on free energy
511 of transfer (kcal/mole) ⁵² implemented by the R package Peptides (the Comprehensive R Archive
512 Network repository; <https://journal.r-project.org/archive/2015/RJ-2015-001/RJ-2015-001.pdf>).

513 We used 532 heavy chain CDR3 amino acid sequences from this study and 22,654,256 IGH CDR3
514 sequences from the public database of memory B cell receptor sequences⁵³. The Shapiro–Wilk
515 test was used to determine whether the GRAVY scores are normally distributed. The GRAVY
516 scores from all 532 IGH CDR3 amino acid sequences from this study were used to perform the
517 test and 5,000 GRAVY scores of the sequences from the public database were randomly selected.
518 The Shapiro–Wilk P values were 6.896×10^{-3} and 2.217×10^{-6} for sequences from this study
519 and the public database, respectively, indicating that the data were not normally distributed.
520 Therefore, we used the Wilcoxon nonparametric test to compare the samples, which indicated a
521 difference in hydrophobicity distribution ($P = 5 \times 10^{-6}$) (Extended data Fig.7).

522

523 Heatmap of log₂ relative fold change in EC₅₀ against the indicated RBD mutants for antibody
524 clonal pairs obtained at 1.3 and 6.2 months (Fig.3e and Extended data Fig. 8k) was created with R
525 pheatmap package (<https://github.com/raivokolde/pheatmap>) using Euclidean distance and
526 Ward.2 clustering method.

527

528 **Biopsies and Immunofluorescence**

529 Endoscopically obtained mucosal biopsies were formalin fixed and paraffin embedded. Sections
530 (5µm) were cut, dewaxed in xylene, and rehydrated in graded alcohol and phosphate-buffered
531 saline (PBS). Heat-induced epitope retrieval was performed in target retrieval solution (Dako,
532 S1699) using a commercial pressure cooker. Slides were then cooled to room temperature, washed
533 in PBS and permeabilized for 30 minutes in 0.1% tritonX-100 in PBS. Non-specific binding was
534 blocked with 10% goat serum (Invitrogen, 50062Z) for 1 hour at room temperature. Sections were
535 then incubated with a combination of primary antibodies diluted in blocking solution overnight at

536 4°C. Slides were washed 3 times in PBS and then incubated in secondary antibody and 4',6-
 537 diamidino-2-phenylindole (1ug/mL) for 1 hour at room temperature. Sections were washed in PBS
 538 3 times and then mounted with Fluoromount-G (Electron Microscopy Sciences, 1798425).
 539 Controls included, omitting primary antibody (no primary 995 control), or substituting primary
 540 antibodies with non-reactive antibodies of the same isotype (isotype control). A Nikon Eclipse Ni
 541 microscope and digital SLR camera (Nikon, DS-Qi2) was used to visualize and image the tissue.
 542
 543 The antibody used to stain sections for N protein was raised in rabbits against SARS-CoV N and
 544 is cross-reactive with SARS-CoV-2 N protein ⁵⁴.
 545

| Antigen | Clone | Vendor | Catalogue number | Host species | Conjugate | Dilution |
|--|------------|---|------------------|--------------|-----------------|----------|
| ACE2 | Polyclonal | Abcam | ab15348 | rabbit | unconjugated | 1:1000 |
| EPCAM | SPM491 | GeneTex | GTX34693 | mouse | unconjugated | 1:100 |
| SARS-CoV-2 nucleocapsid | Polyclonal | Spiegel, M. <i>et al.</i> ⁵⁴ | N/A | rabbit | unconjugated | 1:2000 |
| No known specificity (isotype control) | Polyclonal | Abcam | ab37415 | rabbit | unconjugated | variable |
| Yeast GAL4 (isotype control) | 15-6E10A7 | Abcam | ab170190 | mouse | unconjugated | variable |
| Mouse IgG H&L | Polyclonal | Abcam | ab150116 | goat | Alexa Fluor 594 | 1:1000 |

| | | | | | | |
|----------------|------------|-------|----------|------|-----------------|--------|
| Rabbit IgG H&L | Polyclonal | Abcam | ab150077 | goat | Alexa Fluor 488 | 1:1000 |
|----------------|------------|-------|----------|------|-----------------|--------|

546

547 **SARS-CoV-2 PCR (intestinal biopsies)**

548 To determine if SARS-CoV-2 RNA is present in the gastrointestinal tract we isolated
549 RNA from endoscopically obtained mucosal biopsies using Direct-zol miniprep kit (Zymo
550 research, Cat. No. R2050). Reverse transcribed cDNA was amplified using 2019-nCov Ruo Kit
551 (IDT) to detect viral nucleocapsid genomic RNA. Amplification of sub-genomic nucleocapsid
552 RNA was done using following primers and probe: sgLeadSARSCov2_F 5'-
553 CGATCTCTTGTAGATCTGTTCTC -3'²⁶, wtN_R4 5' – GGTGAACCAAGACGCAGTAT – 3',
554 wtN_P4 5' – /56-FAM/TAACCAGAA/ZEN/TGGAGAACGCAGTGGG/3IABkFQ/ – 3'.
555 Quantitative PCR was performed using QuantTect probe PCR kit (Qiagen, Cat. No. 204345) under
556 following conditions: 95 15', 95°C 15 sec, 60°C 1 min using the Applied Biosystem QuantStudio
557 6 Flex Real-Time PCR System. Viral RNA was considered detected if the cycle threshold (Ct) for
558 viral primers/probes was <40. Samples from positive wells were column purified and presence of
559 N1 sequences additionally verified by Sanger sequencing.

560

561 **Electron Microscopy and Dual-Axis Tomography**

562 Tissues samples were fixed with 3% glutaraldehyde to meet biosafety requirements. Tissues were
563 rinsed with cold 0.1M sodium cacodylate trihydrate + 5% sucrose and further dissected to block
564 sizes sufficient for embedding and sectioning. Tissues were postfixed for 1 h with cold 2% osmium
565 tetroxide in cacodylate buffer, en bloc stained with 1% aqueous uranyl acetate, dehydrated with
566 acetone and embedded in Epon-Araldite resin (Electron Microscopy Sciences). Samples were flat-
567 embedded between two Teflon-coated glass microscope slides and the resin polymerized at 60 °C

568 for 24 h. Embedded tissue blocks were observed by light microscopy to ascertain preservation
569 quality and select regions of interest (i.e., apical epithelium). Blocks were extracted with a scalpel
570 and glued to plastic sectioning stubs prior to sectioning. Semi-thin (150 nm) serial sections were
571 cut with a UC6 ultramicrotome (Leica Microsystems) using a diamond knife (Diatome, Ltd.
572 Switzerland). Sections were placed on formvar-coated copper-rhodium slot grids (Electron
573 Microscopy Sciences) and stained with 3% uranyl acetate and lead citrate. Colloidal gold particles
574 (10 nm) were placed on both surfaces of the grids to serve as fiducial markers for tomographic
575 image alignment. Grids were placed in a dual-axis tomography holder (Model 2010, E.A.
576 Fischione Instruments, Export PA) and imaged with a Tecnai G2 T12 transmission electron
577 microscope (120 KeV; ThermoFisher Scientific). Images were recorded with a 2k x 2k CCD
578 camera (XP1000; Gatan, Pleasanton, CA). Tomographic tilt series and large-area montages were
579 acquired automatically using the SerialEM software package ⁵⁵. For dual-axis tomography, images
580 were collected at 1° intervals as samples were tilted +/- 62°. The grid was then rotated 90° and a
581 second tilt-series was acquired about the orthogonal axis. Tomograms were calculated, analyzed
582 and modeled using the IMOD software package ^{56,57} on MacPro and iMac Pro computers (Apple,
583 Inc).

584

585 Presumptive SARS-CoV-2 virions were identified from tomographic reconstructions of tissue
586 samples by observing structures resembling virions described in cryo-electron tomography studies
587 of purified SARS-CoV-2 and SARS-CoV-2 in infected cells ⁵⁸⁻⁶¹. We used the following criteria
588 for SARS-CoV-2 virion identification in tissues: (i) Structures that were spherical in 3D and not
589 continuous with other adjacent structures with ~60-120 nM diameters, (ii) Spherical structures
590 with densities corresponding to a distinct membrane bilayer, internal puncta consistent with

591 ribonucleoproteins⁵⁸, and densities corresponding to surface spikes on the external peripheries of
592 the spheres.

593

594 **Competing interests:** The Rockefeller University has filed a provisional patent application in
595 connection with this work on which D.F.R. and M.C.N. are inventors (US patent 63/021,387).

596

597 **Data availability statement:** Data are provided in SI Tables 1-7. The raw sequencing data
598 associated with Figure 2 has been deposited at Github (<https://github.com/stratust/igpipeline>). This
599 study also uses data from “A Public Database of Memory and Naive B-Cell Receptor Sequences”
600 (<https://doi.org/10.5061/dryad.35ks2>), PDB (6VYB and 6NB6) and from “High frequency of
601 shared clonotypes in human B cell receptor repertoires” ([https://doi.org/10.1038/s41586-019-](https://doi.org/10.1038/s41586-019-0934-8)
602 0934-8)

603

604 **Code availability statement:** Computer code to process the antibody sequences is available at
605 GitHub (<https://github.com/stratust/igpipeline>).

606

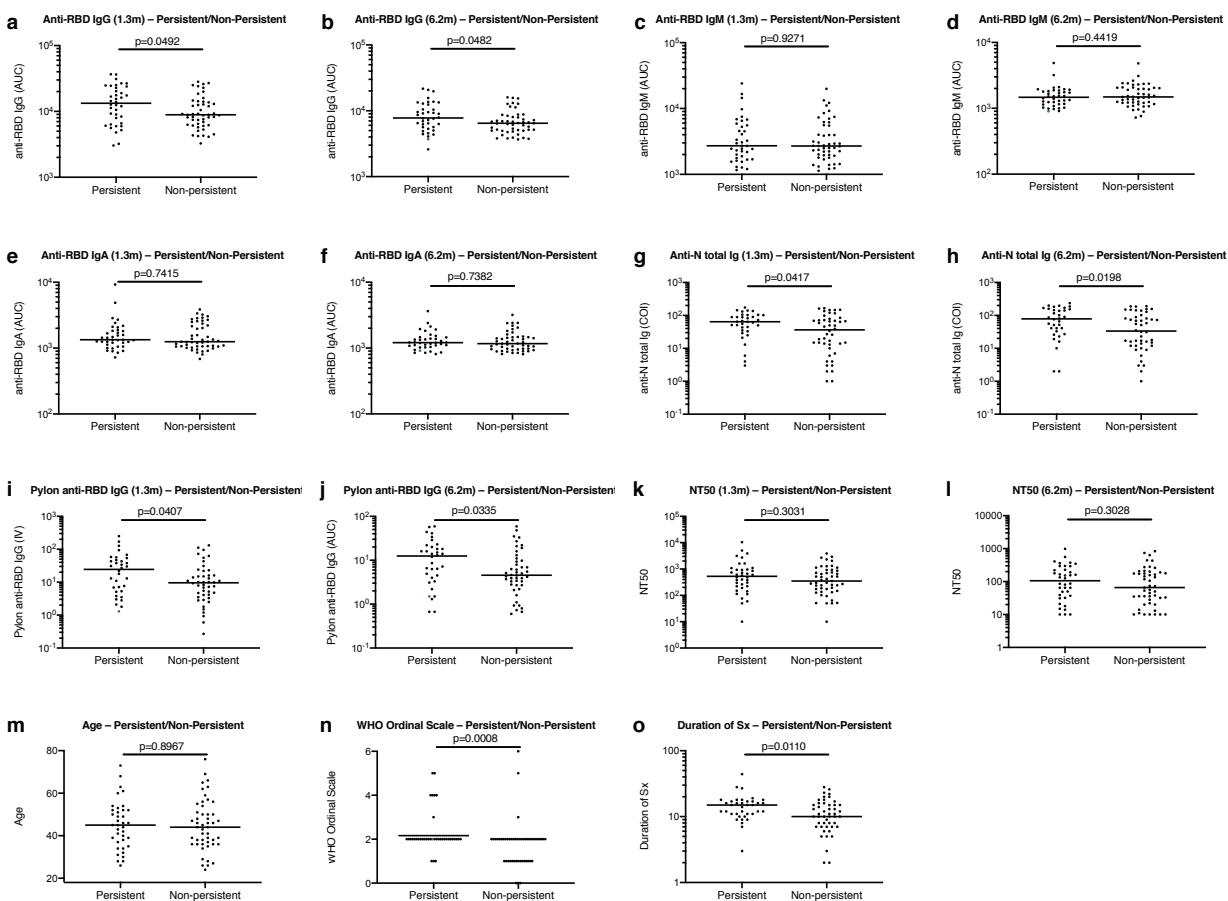
607 **Acknowledgements:** We thank all study participants who devoted time to our research; Drs. Barry
608 Coller and Sarah Schlesinger, the Rockefeller University Hospital Clinical Research Support
609 Office and nursing staff. Mayu Okawa Frank and Robert B. Darnell for SARS-CoV-2 saliva PCR
610 testing. Charles M. Rice and all members of the M.C.N. laboratory for helpful discussions and
611 Maša Jankovic for laboratory support. This work was supported by NIH grant P01-AI138398-S1
612 (M.C.N. and P.J.B.) and 2U19AI111825 (M.C.N.); the Caltech Merkin Institute for Translational
613 Research and P50 AI150464-13 (P.J.B.), George Mason University Fast Grant (D.F.R. and P.J.B.)

614 and the European ATAC consortium EC 101003650 (D.F.R.); R37-AI64003 to P.D.B.;
615 R01AI78788 to T.H.; We thank Dr. Jost Vielmetter and the Protein Expression Center in the
616 Beckman Institute at Caltech for expression assistance. Electron microscopy was performed in the
617 Caltech Beckman Institute Resource Center for Transmission Electron Microscopy. C.O.B. is
618 supported by the HHMI Hanna Gray and Burroughs Wellcome PDEP fellowships. C.G. was
619 supported by the Robert S. Wennett Post-Doctoral Fellowship, in part by the National Center for
620 Advancing Translational Sciences (National Institutes of Health Clinical and Translational Science
621 Award program, grant UL1 TR001866), and by the Shapiro-Silverberg Fund for the Advancement
622 of Translational Research. P.D.B. and M.C.N. are Howard Hughes Medical Institute Investigators.
623

624 **Author Contributions:** C.G., P.D.B., P.J.B., T.H., S.B. and M.C.N. conceived, designed and
625 analyzed the experiments. D.F.R., M.Caskey. and C.G. designed clinical protocols. Z.W., J.C.C.L.,
626 F.M., S.F., M.T., M.L., A.C., M.J., D.S.B., F.S., Y.W., C.V., C.O.B., K.G., D.J., J.Y. and Z.Z.
627 carried out experiments. A.G. and M.Cipolla produced antibodies. A.H., D.S.B., M.Turroja,
628 K.G.M., M.Tankelevich, C.G. and M.Caskey recruited participants and executed clinical
629 protocols. I.S. processed clinical samples. T.Y.O. performed bioinformatic analysis. C.G, P.D.B.,
630 P.J.B., T.H., S.B. and M.C.N. wrote the manuscript with input from all co-authors.

631

632 Extended Data Figures

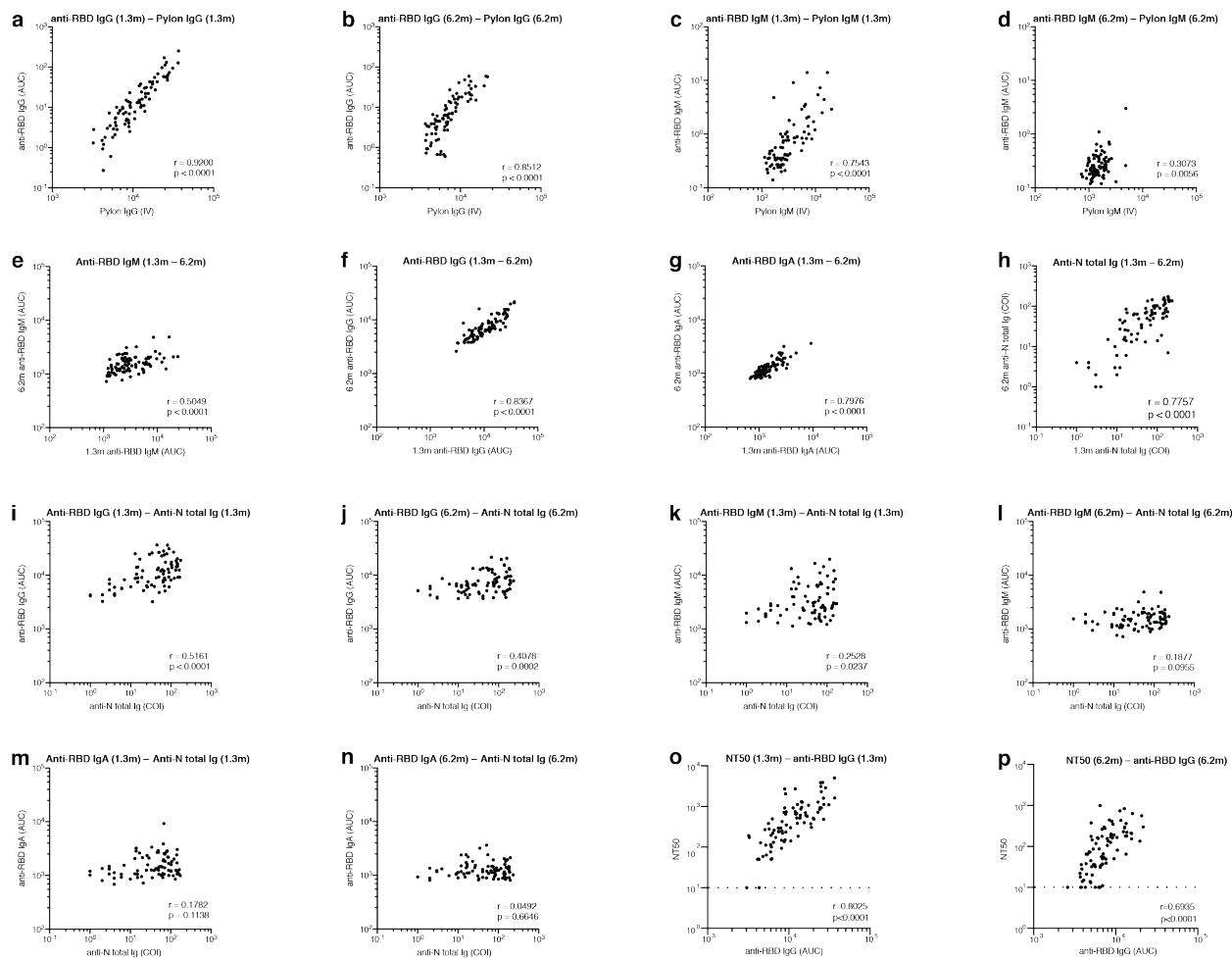


633

634 Extended Data Fig. 1: Clinical correlates of plasma antibody titres.

635 **a**, Normalized AUC anti-RBD IgG titres at 1.3 months for participants with (n=38) or without
636 (n=49) persistent post-acute symptoms. **b**, Normalized AUC anti-RBD IgG titres at 6.2 months for
637 participants with (n=38) or without (n=49) persistent post-acute symptoms. **c**, Normalized AUC
638 anti-RBD IgM titres at 1.3 months for participants with (n=38) or without (n=49) persistent post-
639 acute symptoms. **d**, Normalized AUC anti-RBD IgM titres at 6.2 months for participants with
640 (n=38) or without (n=49) persistent post-acute symptoms. **e**, Normalized AUC anti-RBD IgA titres
641 at 1.3 months for participants with (n=38) or without (n=49) persistent post-acute symptoms. **f**,
642 Normalized AUC anti-RBD IgA titres at 6.2 months for participants with (n=38) or without (n=49)

643 persistent post-acute symptoms. **g**, COI values of anti-N total Ig titres at 1.3 months for participants
644 with (n=38) or without (n=49) persistent post-acute symptoms. **h**, COI values of anti-N total Ig
645 titres at 6.2 months for participants with (n=38) or without (n=49) persistent post-acute symptoms.
646 **i**, IV values of anti-RBD IgG titres at 1.3 months for participants with (n=38) or without (n=49)
647 persistent post-acute symptoms. **j**, IV values of anti-RBD IgG titres at 6.2 months for participants
648 with (n=38) or without (n=49) persistent post-acute symptoms. **k**, NT50 values at 1.3 months for
649 participants with (n=38) or without (n=49) persistent post-acute symptoms. **l**, NT50 values at 6.2
650 months for participants with (n=38) or without (n=49) persistent post-acute symptoms. **m**, Age in
651 years for participants with (n=38) or without (n=49) persistent post-acute symptoms. **n**, Severity
652 of acute infection as assessed by the WHO Ordinal Clinical Progression/Improvement Scale for
653 participants with (n=38) or without (n=49) persistent post-acute symptoms. **o**, Duration of
654 Symptoms during acute infection for participants with (n=38) or without (n=49) persistent post-
655 acute symptoms. Horizontal bars indicate median values. Statistical significance was determined
656 using Mann–Whitney U-tests.

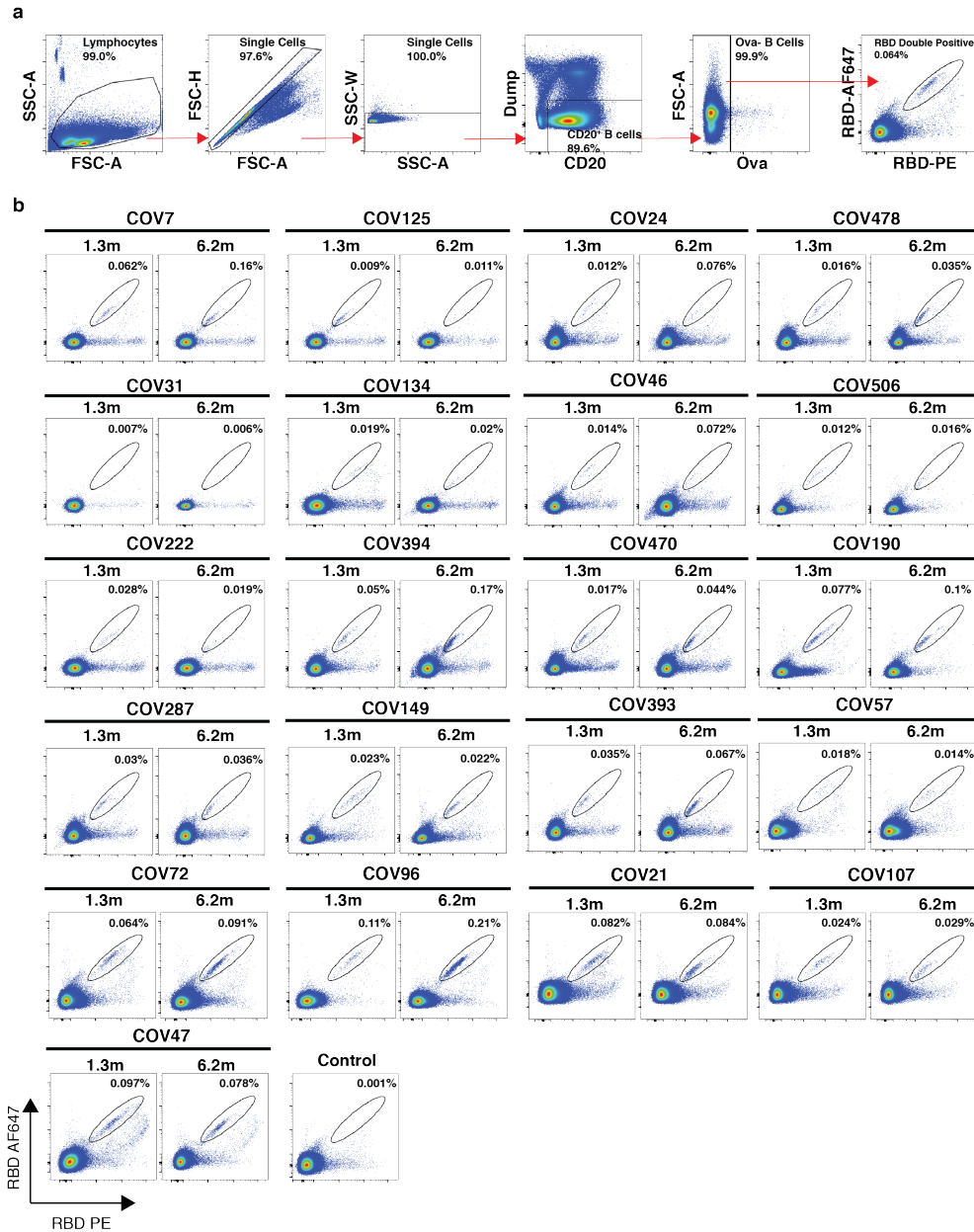


657

658 **Extended Data Fig. 2: Correlations of plasma antibody measurements.**

659 **a**, Normalized AUC for IgG anti-RBD plotted against Pylon IgG anti-RBD index values at 1.3
 660 months. **b**, Normalized AUC for IgG anti-RBD plotted against Pylon IgG anti-RBD index
 661 values at 6.2 months. **c**, Normalized AUC for IgM anti-RBD plotted against Pylon IgM anti-RBD
 662 index values at 1.3 months. **d**, Normalized AUC for IgM anti-RBD plotted against Pylon IgM anti-RBD
 663 index values at 6.2 months. **e**, Normalized AUC for IgM anti-RBD at 6.2 months plotted against
 664 IgM anti-RBD at 1.3 months. **f**, Normalized AUC for IgG anti-RBD at 6.2 months plotted against
 665 IgG anti-RBD at 1.3 months. **g**, Normalized AUC for IgA anti-RBD at 6.2 months plotted against
 666 IgA anti-RBD at 1.3 months. **h**, COI values for anti-N total Ig titres at 6.2 months plotted against

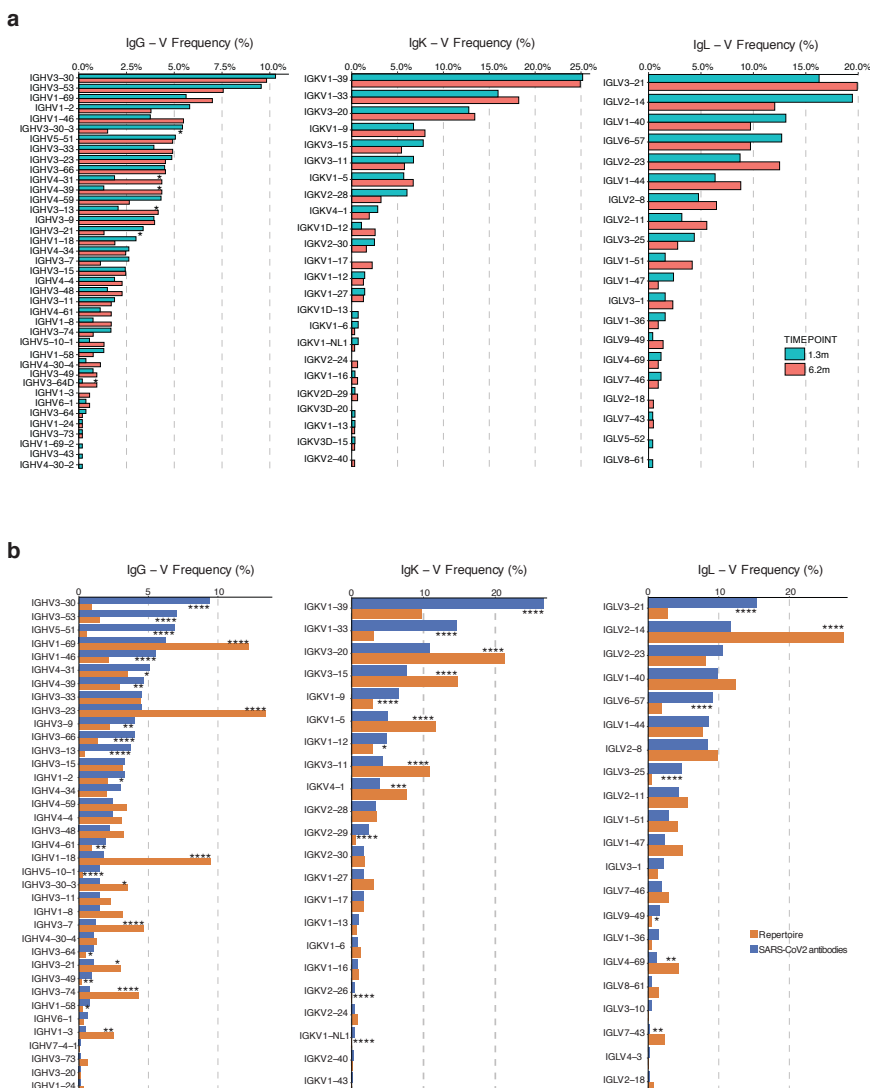
667 anti-N total Ig titres at 1.3 months. **i**, Anti-RBD IgG titres at 1.3 months plotted against anti-N total
668 Ig titres at 1.3 months. **j**, Anti-RBD IgG titres at 6.2 months plotted against anti-N total Ig titres at
669 6.2 months. **k**, Anti-RBD IgM titres at 1.3 months plotted against anti-N total Ig titres at 1.3
670 months. **l**, Anti-RBD IgM titres at 6.2 months plotted against anti-N total Ig titres at 6.2 months.
671 **m**, Anti-RBD IgA titres at 1.3 months plotted against anti-N total Ig titres at 1.3 months. **l**, Anti-
672 RBD IgA titres at 6.2 months plotted against anti-N total Ig titres at 6.2 months. **o**, NT50 values at
673 1.3 months plotted against anti-RBD IgG titres at 1.3 months. **p**, NT50 values at 6.2 months plotted
674 against anti-RBD IgG titres at 6.2 months. The r and p values were determined by two-tailed
675 Spearman's correlations.



676

677 **Extended Data Fig. 3: Flow cytometry.**

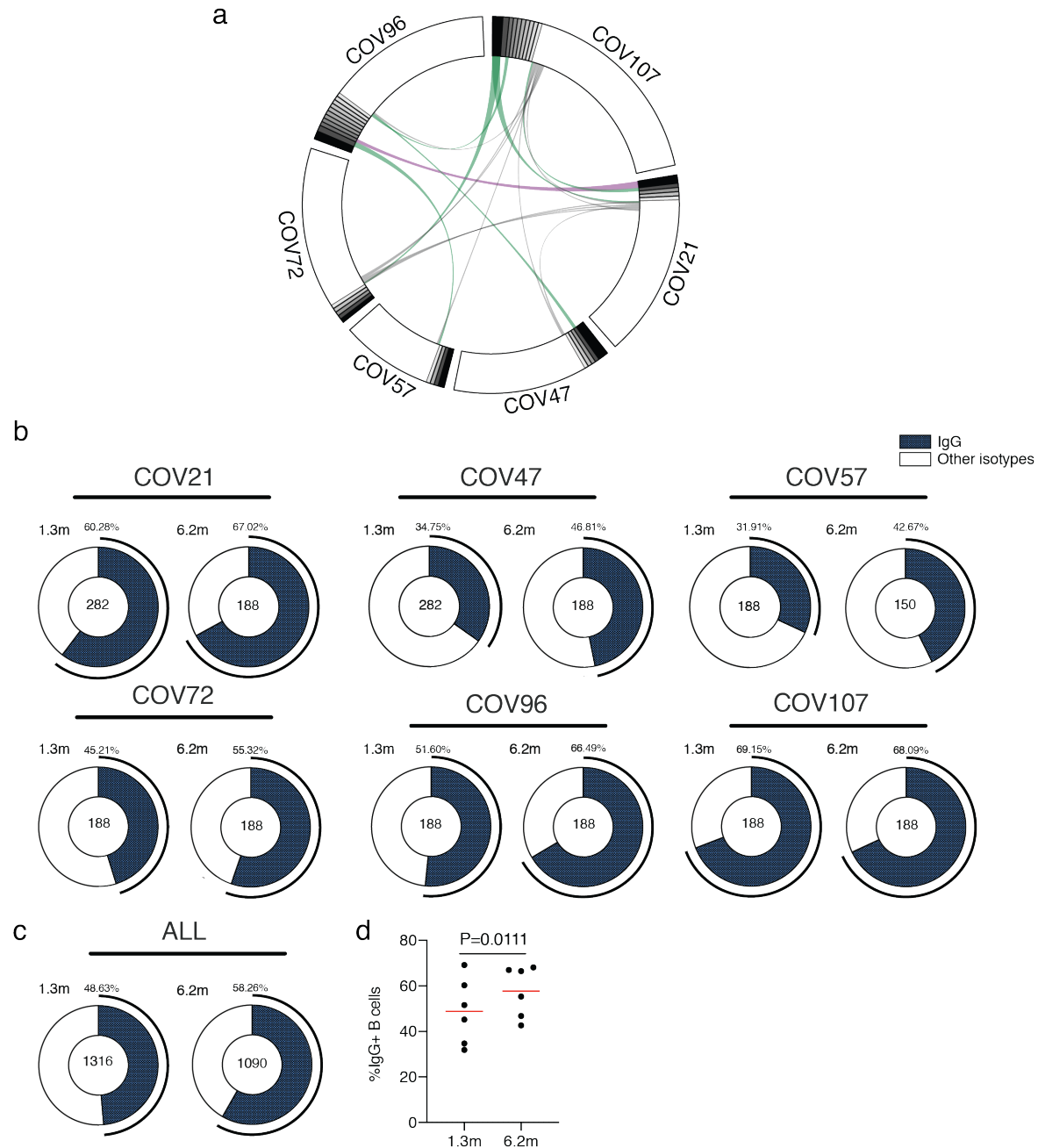
678 **a**, Gating strategy used for cell sorting. Gating was on singlets that were CD20+ and
 679 CD3-CD8-CD16-Ova-. Sorted cells were RBD-PE+ and RBD-AF647+. **b**, Flow cytometry
 680 showing the percentage of RBD-double positive memory B cells from month 1.3 or month 6 post-
 681 infection in 21 randomly selected patients.



682

683 **Extended Data Fig. 4: Frequency distributions of human V genes.**

684 **a**, Two-sided binomial tests were used to compare the frequency distributions of human V genes
 685 of anti-SARS-CoV-2 antibodies from donors at 1.3 months to 6.2 months ¹. **b**, Two-sided binomial
 686 tests were used to compared the frequency distributions of human V genes of anti-SARS-CoV-2
 687 antibodies from this study to sequence from *C. Soto et al.* ⁴⁹.



688

689 **Extended Data Fig. 5: Circos plots and IgG positive RBD specific B cells**

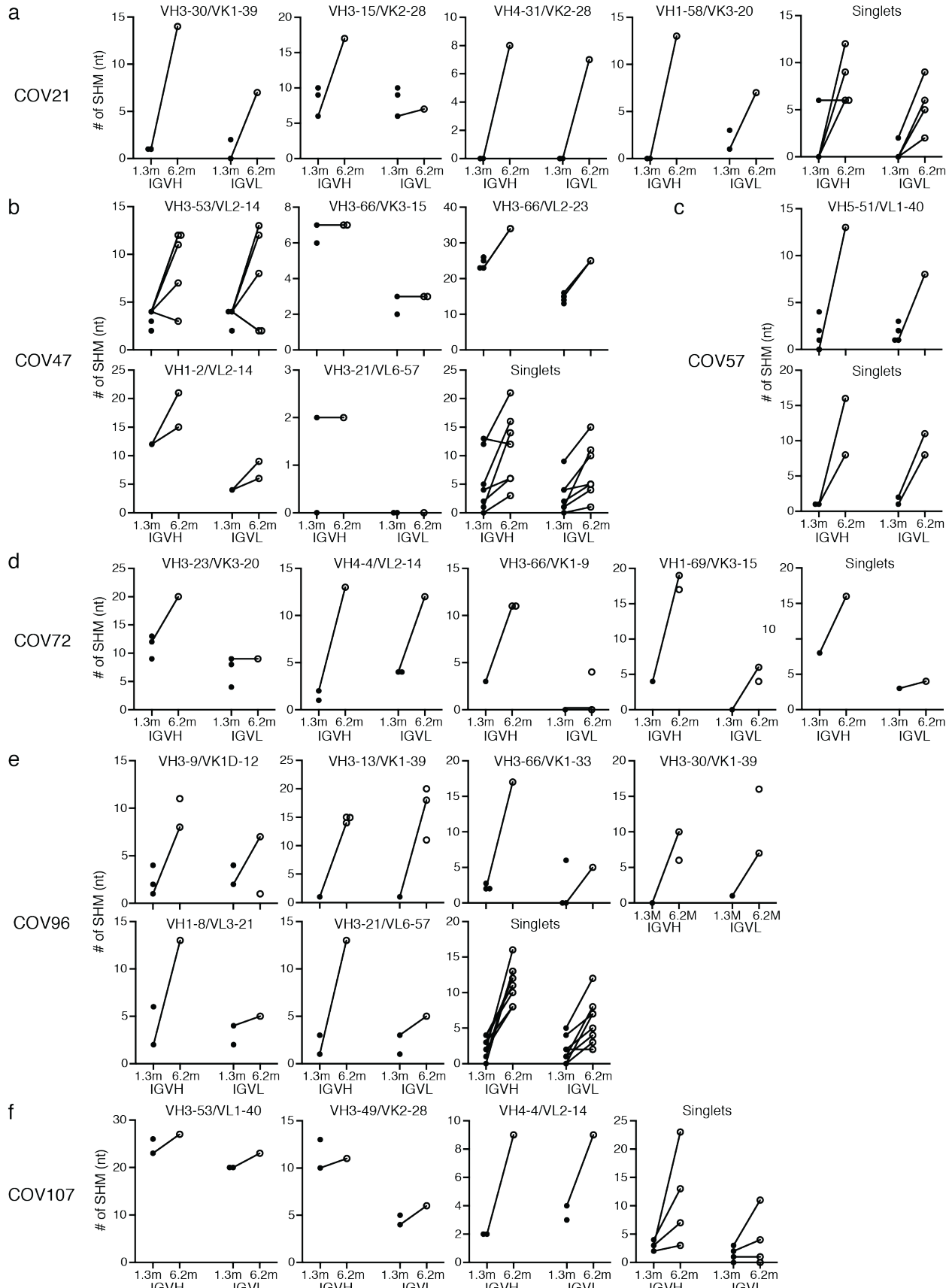
690 **a**, Sequences from all six individuals with clonal relationships depicted as in Figure 2d.

691 Interconnecting lines indicate the relationship between antibodies that share V and J gene segment

692 sequences at both IGH and IGL. Purple, green and grey lines connect related clones, clones and

693 singles, and singles to each other, respectively. **b**, For each patient, the number of IgG heavy chain

694 sequences (black) analyzed from six individuals at month 1.3 (left panel) or month 6.2 post-
695 infection (right panel). The number in the inner circle indicates the number of cells that was sorted
696 for each individual denoted above the circle. **c**, The same as b but showing the all 6 patients
697 combined data. **d**, The comparison of the percentage of IgG positive B cells from six individuals
698 at month 1.3 or month 6.2 post-infection. The horizontal bars indicate the mean. Statistical
699 significance was determined using paired t test.

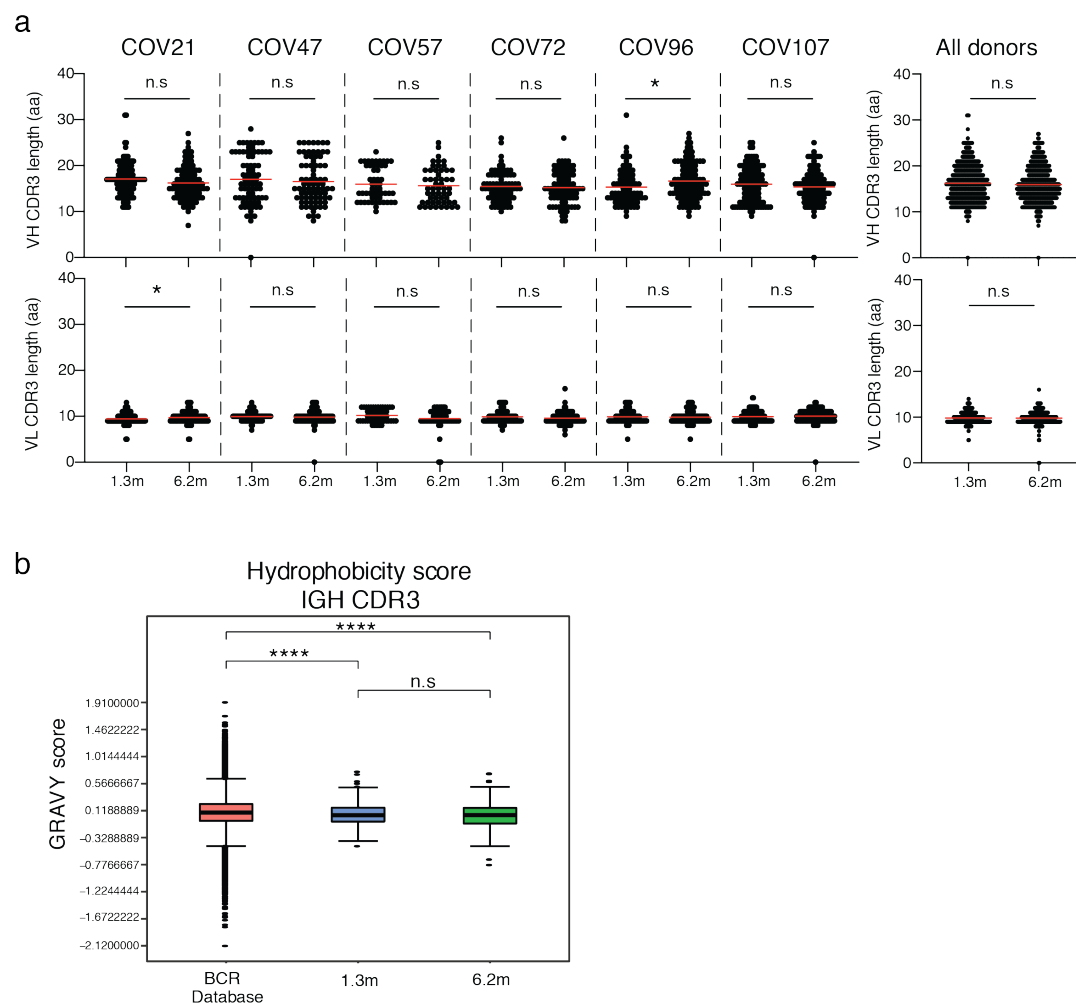


700

701 **Extended Data Fig. 6: Analysis of antibody somatic hypermutation of persisting clones.**

702 Number of somatic nucleotide mutations in both the IGVH and IGVL of persisting clones found
703 at month 1.3 (solid circles) and month 6.2 time points (open circles) in patients (a) COV21, (b)
704 COV47, (c) COV57, (d) COV72, (e) COV96, and (f) COV107. The VH and VL gene usage of
705 each clonal expansion is indicated above the graphs, or are indicated as “Singlets” if the persisting
706 sequence was isolated only once at both time points. Connecting line indicates the SHM of the
707 clonal pairs that were expressed as a recombinant mAbs.

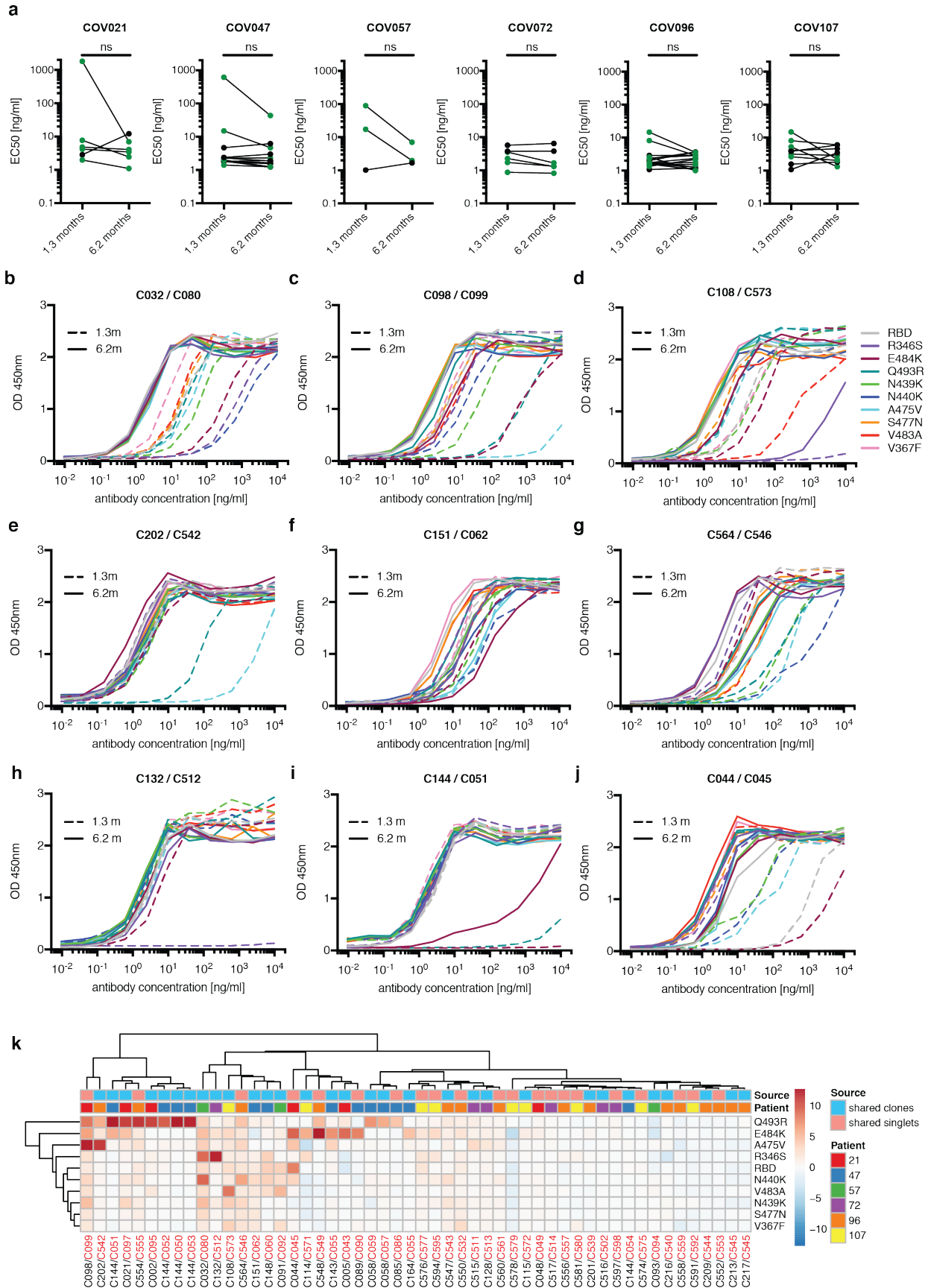
708



709

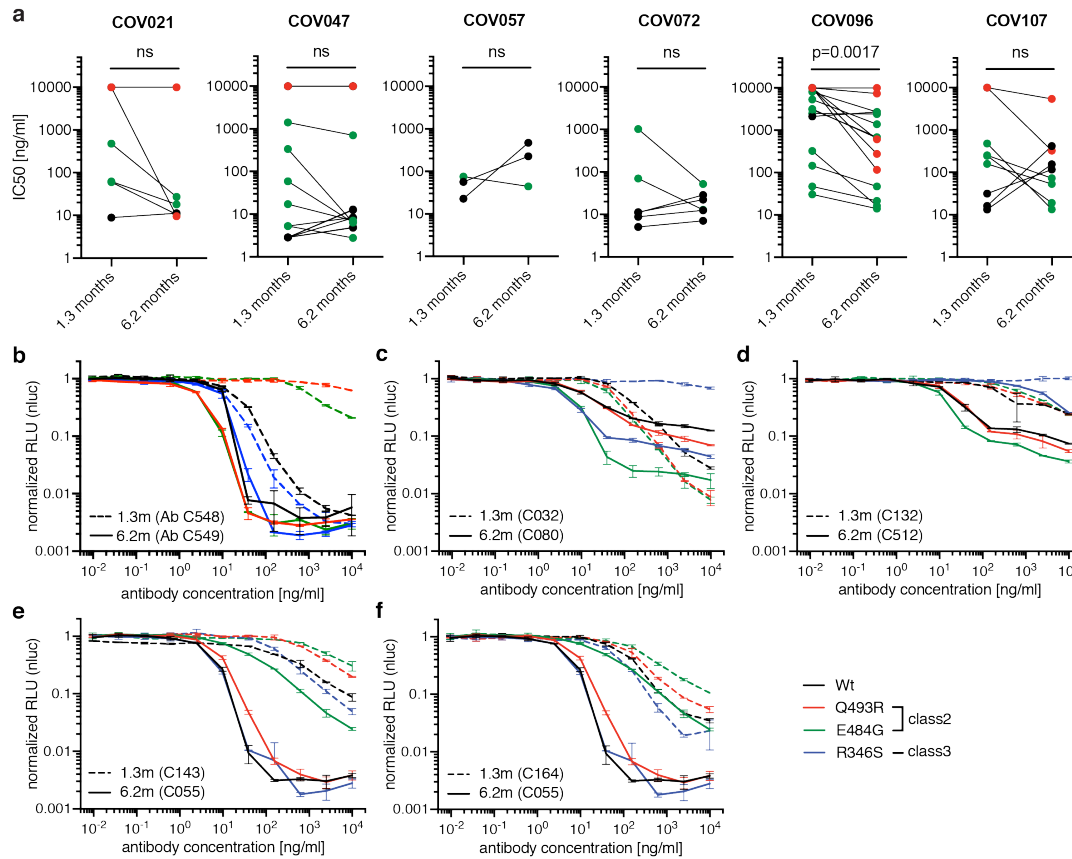
710 **Extended Data Fig. 7: Analysis of CDR3 length and hydrophobicity.**

711 **a**, For each individual, the number of the amino acid length of the CDR3s at the IGVH and IGVL
 712 is shown. The horizontal bars indicate the mean. The number of antibody sequences (IGVH and
 713 IGVL) evaluated for each participant are $n = 90$ (COV21), $n = 78$ (COV47), $n = 53$ (COV57), $n =$
 714 87 (COV72), $n = 104$ (COV96), $n = 120$ (COV107). Right panel show all antibodies combined (n
 715 $= 532$ for both IGVH and IGVL). **b**, Distribution of the hydrophobicity GRAVY scores at the
 716 IGH CDR3 in antibody sequences from this study compared to a public database (see Methods for
 717 statistical analysis). The box limits are at the lower and upper quartiles, the centre line indicates
 718 the median, the whiskers are $1.5\times$ interquartile range and the dots represent outliers.



720 **Extended Data Fig. 8: ELISA of wt/mutant RBD for mAbs.**

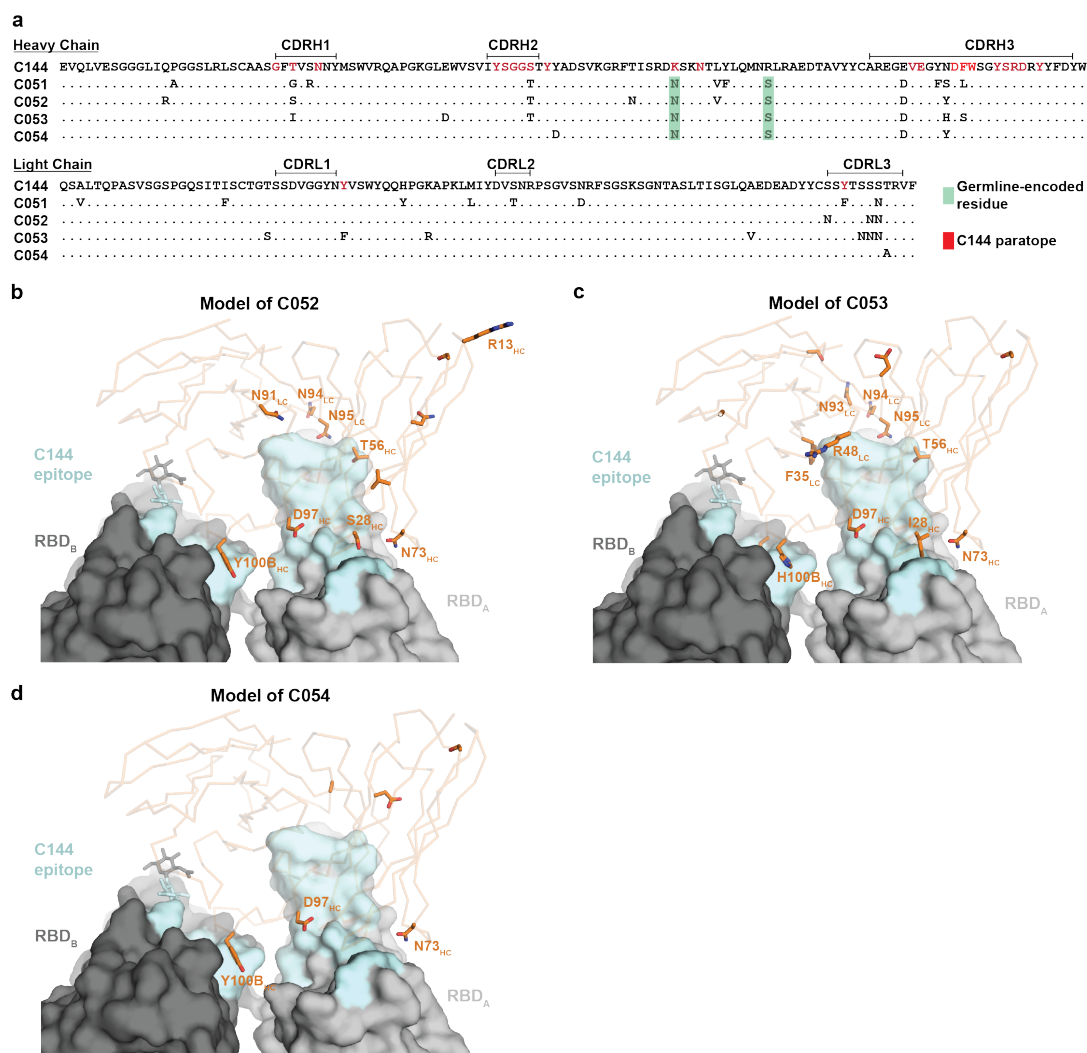
721 **a**, EC₅₀ values for binding to wild type RBD of shared singlets and shared clones of mAbs
722 obtained at the initial 1.3 and 6.2 months follow-up visit, divided by patient. Lines connect shared
723 singlets/clones. mAbs with improved EC₅₀ at 6.2 months follow-up visit are highlighted in green,
724 remaining mAbs are shown in black. Statistical significance was determined using Wilcoxon
725 matched-pairs signed rank test. **b-j**, Graphs show ELISA binding curves for different antibodies
726 obtained at 1.3 months (dashed lines) and their clonal relatives obtained after 6.2 months (solid
727 lines) binding to wild type, R346S, E484K, Q493R, N439K, N440K, A475V, S477N, V483A and
728 V367F RBDs (colors as indicated). Antibody IDs of pairs as indicated on top of panels (1.3m /
729 6.2m). **k**, Heat map shows log₂ relative fold change in EC₅₀ against the indicated RBD mutants
730 for 52 antibody clonal pairs obtained at 1.3 (black) and 6.2 months (red). The clonal and participant
731 origin for each antibody pair is indicated above.



732

733 **Extended Data Fig. 9: neutralization of wt/mutant RBD pseudotypes by mAbs.**

734 **a**, IC50 values of shared singlets and shared clones of mAbs obtained at the initial 1.3- and 6.2-
 735 months follow-up visit, divided by patient. Lines connect shared singlets/clones. mAbs with
 736 undetectable IC50 at 1.3 months are plotted at 10 μ g/ml and are highlighted in red, mAbs with
 737 improved IC50 at 6.2 months follow-up visit are highlighted in green, remaining mAbs are shown
 738 in black. Statistical significance was determined using Wilcoxon matched-pairs signed rank test.
 739 **b-f**, The normalized relative luminescence values for cell lysates of 293T Ace2 cells 48 hpi with
 740 SARS-CoV-2 pseudovirus harboring wt RBD or RBD-mutants (wt, Q493R, E484G and R346S
 741 RBD shown in black, red, green and blue, respectively) in the presence of increasing
 742 concentrations of mAbs obtained at the 1.3 months initial visit (1.3m, dashed lines) and their shared
 743 clones/singlets at the 6.2 follow-up visit (6.2m, continuous lines). Antibody IDs as indicated.

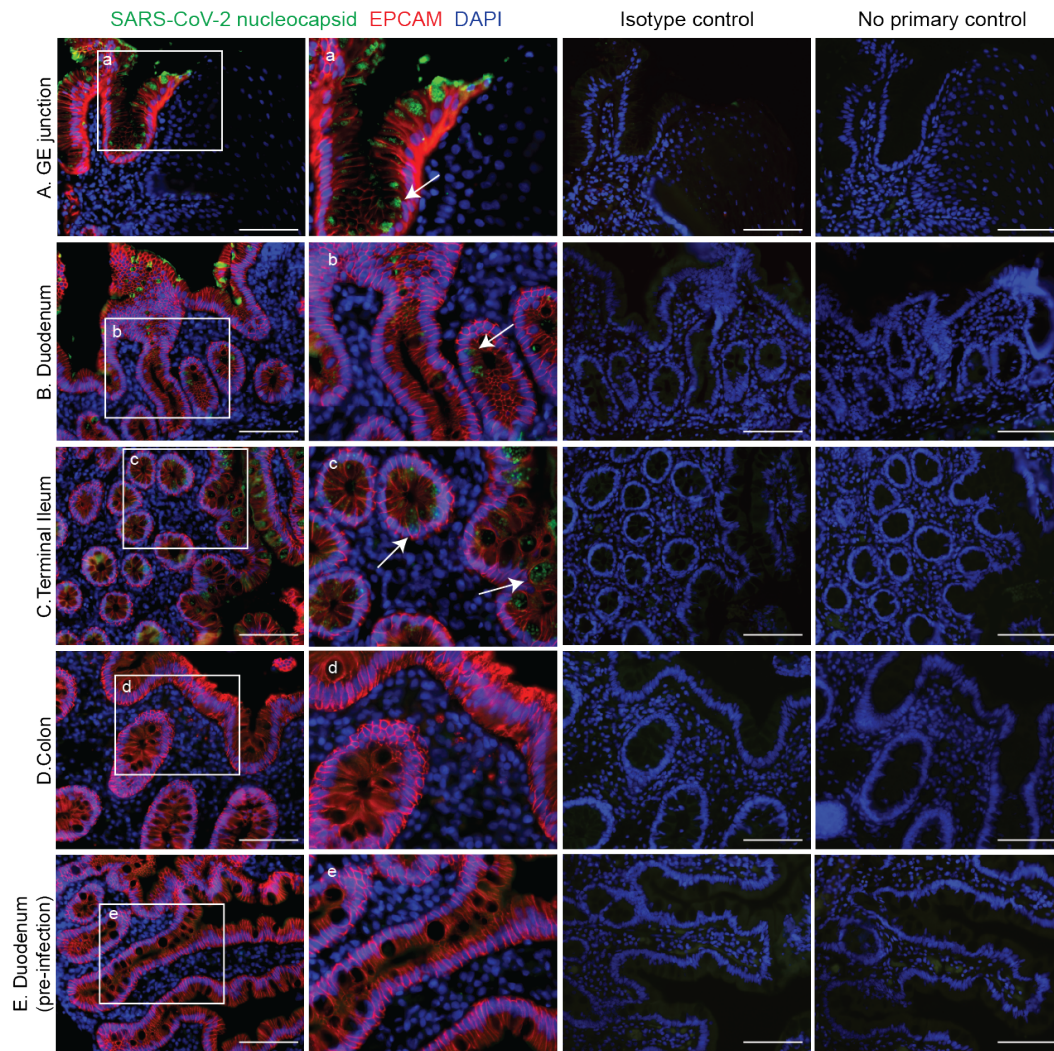


744

745 **Extended Data Fig. 10: C51 alignment and binding projection**

746 **a**, VH and VL amino acid sequence alignment of C144 and derivative antibodies C051, C052,
 747 C053 and C054. Germline-encoded residues are highlighted in green. Residues in the proximity
 748 of RBD-binding C144 paratope are highlighted in red.

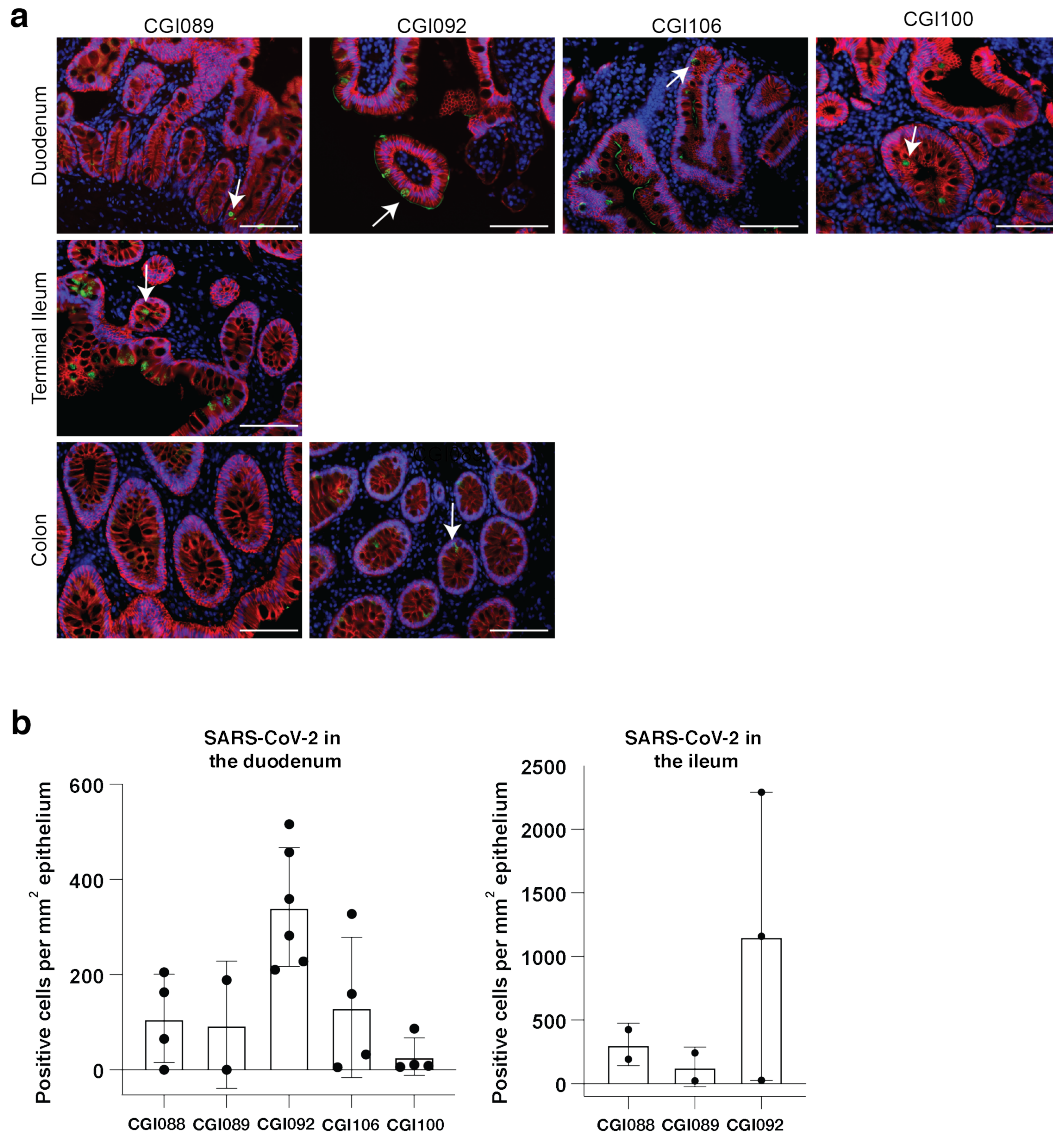
749 **b-e**, Surface representation of two adjacent “down” RBDs (RBD_A and RBD_B) on a spike trimer
 750 with the C144 epitope on the RBDs highlighted in cyan and positions of amino acid mutations that
 751 accumulated in **b**, C052. **c**, C053 and **d**, C054 compared to the parent antibody C144 highlighted
 752 as stick side chains on a C α atom representation. The C052, C053 and C054 interactions with two
 753 RBDs was modeled based on a cryo-EM structure of C144 Fab bound to spike trimer¹⁶.



754

755 **Extended Data Fig. 11: SARS-CoV-2 antigen in human enterocytes in the gastrointestinal**
756 **tract 3 months post COVID-19**

757 Immunofluorescence images of human gastrointestinal tissue are shown. Staining is for EPCAM
758 (red), DAPI (blue) and SARS-CoV-2 nucleocapsid (green) Samples are derived from intestinal
759 biopsies in the gastrointestinal tract as indicated (A-E). (A-D) are biopsies from participant CGI-
760 088 (Supplementary Table 7) taken 92 days post COVID-19 symptom onset. (E) is a biopsy 27
761 months prior to COVID-19 symptom onset from the same participant CGI-088. Arrows indicate
762 enterocytes with detectable SARS-CoV-2 antigen. Isotype and no primary controls for each tissue
763 are shown in the last two columns. White scale bar corresponds to 100 μ m.

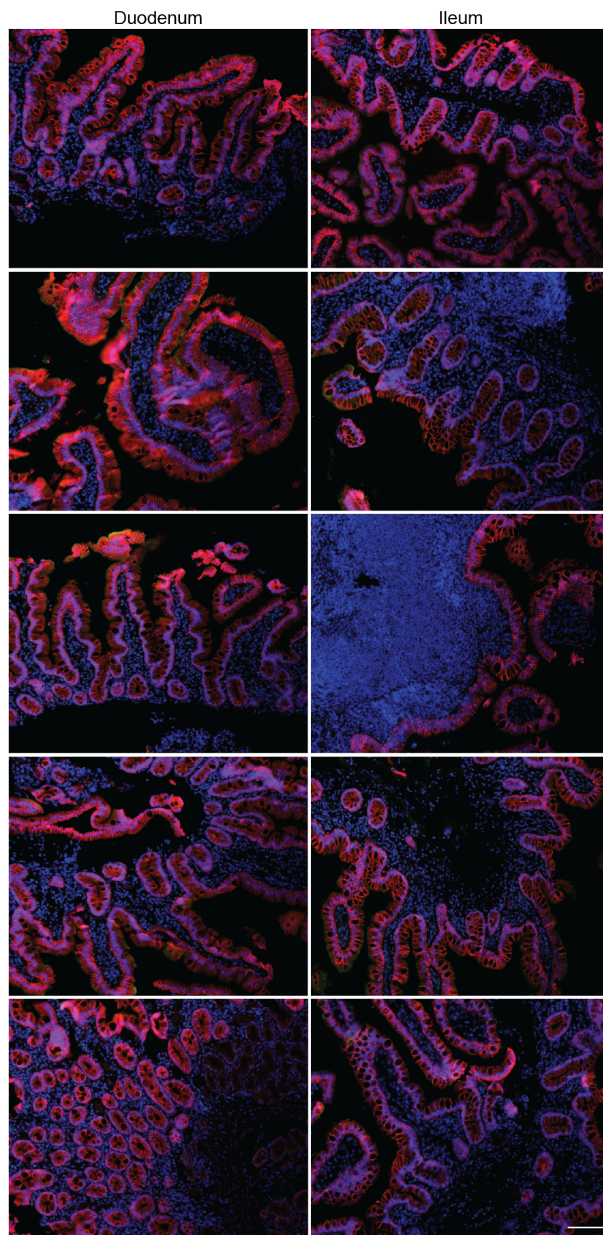


764

765 **Extended Data Fig. 12: SARS-CoV-2 antigen is detectable in different intestinal segments in**
766 **multiple COVID-19 convalescent individuals**

767 **a**, Immunofluorescence (IF) images of biopsy samples in the gastrointestinal tract in different
768 individuals are shown. Staining is for EPCAM (red), DAPI (blue) and SARS-CoV-2 nucleocapsid
769 (green). Samples are derived from intestinal biopsies from 4 participants (CGI089, CGI092,
770 CGI100 and CGI106) taken at least 3 months after COVID-19 infection. Arrows indicate
771 enterocytes with detectable SARS-CoV-2 antigen. White scale bar corresponds to 100 μ m. **b**,

772 Quantification of SARS-CoV-2 positive cells by immunofluorescence. The number of cells
773 staining positive for the nucleocapsid protein (N) of SARS-CoV-2 per mm² of intestinal epithelium
774 is shown. The graphs show biopsy samples from the indicated individuals of the duodenum (left)
775 and terminal ileum (right), respectively. Black dots represent the number of available biopsy
776 specimen for each individual from the respective intestinal segment. Boxes represent median
777 values and whiskers the 95 % CI.



778 EPCAM SARS-CoV-2 nucleocapsid DAPI

779 **Extended Data Fig. 13: Pre-COVID-19 historic control individuals show no detectable**
780 **SARS-CoV-2 antigen by immunofluorescence**

781 Immunofluorescence images of biopsy samples in the gastrointestinal tract obtained from 10
782 different individuals between January 2018 and October 2019 are shown. Staining is for EPCAM
783 (red), DAPI (blue) and SARS-CoV-2 nucleocapsid (green). White scale bar corresponds to 100
784 μm .

785

791 **Supplementary Table 3: Antibody sequences from 1.3 and 6.2 month time point is provided**
 792 **as a separate Excel file.**

793 **Supplementary Table 4: Sequences of the cloned monoclonal antibodies is provided as a**
 794 **separate Excel file.**

795 **Supplementary Table 5: Half maximal effective concentrations (EC50s) of the monoclonal**
 796 **antibodies is provided as a separate Excel file.**

797 **Supplementary Table 6: Inhibitory concentrations of the monoclonal antibodies is provided**
 798 **as a separate Excel file.**

Table 7. Gastrointestinal cohort participant characteristics

| Patient ID | Baseline patient characteristics | | | | | | Gastrointestinal endoscopy | | | SARS-CoV-2 in the intestine | | | | | COVID-19 history | | | | | | |
|------------|----------------------------------|-------------|-----|-------|--------------|---|-----------------------------|------------------|-------------------|-----------------------------|--|-------|---|---------|--|------------------------------|-----------------------------------|---|---------------------------------------|----------------------------------|-----|
| | Case/control | Age (years) | Sex | Race | Ethnicity | Pertinent medical history/comorbidities § | Indication | Procedure type § | Date of procedure | SARS-CoV-2 | SARS-CoV-2 nucleocapsid (N) antigen by immunofluorescence (IF) | | SARS-CoV-2 rPCR from intestinal biopsy samples | | Positive nasopharyngeal SARS-CoV-2 PCR | Positive SARS-CoV-2 serology | Symptom onset to GI biopsy (days) | Positive nasopharyngeal PCR to GI biopsy (days) | Acute disease severity by WHO (0-5) ¶ | COVID-19 associated GI symptoms* | |
| | | | | | | | | | | | Duodenum | Ileum | Corona virus-like particles by electron microscopy (EM) | Genomic | Subgenomic | | | | | | |
| CG886 | case | 52 | M | White | Non-Hispanic | seasonal allergic asthma | GERD | ESD/COLO | June 2020 | Negative | + | + | + | - | - | March 2020 | May 2020 | 87 | 84 | 2 | N |
| CG889 | case | 87 | M | AA | Non-Hispanic | MM, HTN | IBA | ESD/COLO | July 2020 | Negative | + | + | - | - | March 2020 | July 2020 | N/A | 106 | 2 | N | |
| CG890 | case | 73 | M | White | Hispanic | gout, HTN, prostate Cx | CRC screen, GERD | ESD/COLO | July 2020 | Negative | - | - | N/A | - | March 2020 | N/A | 119 | 112 | 2 | N | |
| CG891 | case | 40 | F | White | Non-Hispanic | asthma | bowel changes | ESD/COLO | July 2020 | Negative | - | - | N/A | - | N/A | May 2020 | N/A | N/A | N/A | 2 | N |
| CG892 | case | 70 | M | White | Non-Hispanic | HTN, HLD | CRC screen, GERD | ESD/COLO | July 2020 | Negative | + | + | - | - | April 2020 | August 2020 | N/A | 105 | 2 | Y | |
| CG893 | case | 48 | F | N/A | Hispanic | Ironyalytia, PUD, OA, psoriasis | PUD | EGD | July 2020 | Negative | - | - | N/A | - | N/A | May 2020 | 121 | N/A | N/A | 2 | Y |
| CG894 | case | 30 | M | White | Non-Hispanic | IBD (Crohn) | IBD (Crohn) | ESD/COLO | August 2020 | Negative | - | - | N/A | - | April 2020 | N/A | N/A | 113 | 2 | N | |
| CG895 | case | 27 | F | N/A | Hispanic | allergic rhinitis, GERD | IBS | ESD/COLO | August 2020 | Negative | - | - | N/A | - | April 2020 | N/A | N/A | 130 | 2 | N | |
| CG896 | case | 63 | M | White | Hispanic | prostate Cx, ESRD, DM, HTN | Rectal bleeding | COLO | August 2020 | Negative | N/A | - | N/A | - | April 2020 | N/A | N/A | 148 | 5 | N | |
| CG897 | case | 28 | M | White | Non-Hispanic | IBD (Crohn) | IBD (Crohn) | COLO | August 2020 | Negative | N/A | - | N/A | - | March 2020 | June 2020 | N/A | 99 | 1 | N | |
| CG898 | case | 72 | F | AA | Non-Hispanic | asthma, HTN, HCV | CRC screen | ESD/COLO | September 2020 | Negative | - | - | N/A | - | March 2020 | N/A | N/A | 168 | 2 | Y | |
| CG899 | case | 70 | M | AI | Non-Hispanic | CRC, IBA, CAD | IBA | COLO | September 2020 | Negative | - | - | N/A | - | May 2020 | N/A | 173 | N/A | 2 | Y | |
| CG100 | case | 30 | M | White | Non-Hispanic | DM1, CD | CRC | EGD | September 2020 | Negative | + | N/A | - | - | N/A | May 2020 | N/A | N/A | 1 | N | |
| CG101 | case | 38 | F | White | Non-Hispanic | seasonal allergic asthma | abdominal pain, weight loss | EGD | July 2020 | Negative | + | N/A | - | - | N/A | N/A | N/A | 113 | 2 | Y | |
| Ctrl 1 | control | 79 | F | N/A | N/A | anemia, renal encephalopathy, breast Cx, DM2, HTN | gastroenter follow up | EGD | September 2018 | N/A | - | N/A | N/A | N/A | N/A | N/A | N/A | N/A | N/A | N/A | N/A |
| Ctrl 2 | control | 79 | F | N/A | N/A | Abx, CHF, anemia, HTN, MR | weight loss | EGD | May 2019 | N/A | - | N/A | N/A | N/A | N/A | N/A | N/A | N/A | N/A | N/A | N/A |
| Ctrl 3 | control | 55 | M | N/A | N/A | GERD, EE | abdominal pain | EGD | July 2019 | N/A | - | N/A | N/A | N/A | N/A | N/A | N/A | N/A | N/A | N/A | N/A |
| Ctrl 4 | control | 83 | F | N/A | N/A | asthma, CAD, DM2, HTN, GERD, HLD, OA | dysphagia | EGD | July 2019 | N/A | - | N/A | N/A | N/A | N/A | N/A | N/A | N/A | N/A | N/A | N/A |
| Ctrl 5 | control | 50 | M | N/A | N/A | seasonal allergic asthma, GERD | GERD | EGD | January 2018 | N/A | - | N/A | N/A | N/A | N/A | N/A | N/A | N/A | N/A | N/A | N/A |
| Ctrl 6 | control | 51 | F | N/A | N/A | allergic neuropathy, biopsy tonsillitis | CRC screen | COLO | April 2019 | N/A | N/A | - | N/A | N/A | N/A | N/A | N/A | N/A | N/A | N/A | N/A |
| Ctrl 7 | control | 57 | M | N/A | N/A | GERD, HTN, DM2, psoriasis, GSA, IBS, diverticulosis | abdominal pain | COLO | April 2019 | N/A | N/A | - | N/A | N/A | N/A | N/A | N/A | N/A | N/A | N/A | N/A |
| Ctrl 8 | control | 42 | M | N/A | N/A | none | rectal bleeding | COLO | September 2019 | N/A | N/A | - | N/A | N/A | N/A | N/A | N/A | N/A | N/A | N/A | N/A |
| Ctrl 9 | control | 57 | M | N/A | N/A | spinal cord injury, paraneoplasia, HTN, HLD | CRC screen | COLO | October 2019 | N/A | N/A | - | N/A | N/A | N/A | N/A | N/A | N/A | N/A | N/A | N/A |
| Ctrl 10 | control | 33 | M | N/A | N/A | DM2, obesity, HTN, heart murmur | IBA | COLO | October 2019 | N/A | N/A | - | N/A | N/A | N/A | N/A | N/A | N/A | N/A | N/A | N/A |

AA, African American
 AI, Asian Indian
 § GERD (gastroesophageal reflux disease), CRC (colorectal cancer), IBA (iron deficiency anemia), PUD (peptic ulcer disease), IBD (inflammatory bowel disease), HLD (hyperlipidemia), MR (mitral regurgitation), DM (diabetes mellitus type 2), OA (osteoarthritis), HTN (arterial hypertension), COPD (chronic obstructive pulmonary disease), CAD (coronary artery disease), Abt (abstention), CHF (congestive heart failure), GSA (gastroesophageal sleep apnea), IBS (irritable bowel syndrome), CD (celiac disease), MM (multiple myeloma), ESRD (end stage renal disease), HCV (hepatitis C), EE (eosinophilic esophagitis), MDD (major depressive disorder), Cx (pacemaker)
 ¶ WHO Ordinal Scale for Clinical Impairment, COVID-19 Trial Design Synopses
 * 1 = Persistent fatigue, Symptom abatement, delirium, or 3 other isolated symptoms beyond 8 weeks from symptom onset
 † Onset of symptoms at the time of acute illness including diarrhea, nausea, vomiting

799 **Supplementary Table 7: Gastrointestinal biopsies cohort characteristics**
 800
 801

802 References

- 803 1 Robbiani, D. F. *et al.* Convergent antibody responses to SARS-CoV-2 in convalescent
804 individuals. *Nature* **584**, 437-442, doi:10.1038/s41586-020-2456-9 (2020).
- 805 2 Carfi, A., Bernabei, R., Landi, F. & Gemelli Against, C.-P.-A. C. S. G. Persistent
806 Symptoms in Patients After Acute COVID-19. *JAMA* **324**, 603-605,
807 doi:10.1001/jama.2020.12603 (2020).
- 808 3 American Medical Association. Long-term Health Consequences of COVID-19. 1-2,
809 doi:10.1001/jama.2020.20677 (2020).
- 810 4 Yang, H. S. *et al.* SARS-CoV-2 antibody characterization in emergency department,
811 hospitalized and convalescent patients by two semi-quantitative immunoassays. *Clin*
812 *Chim Acta* **509**, 117-125, doi:10.1016/j.cca.2020.06.004 (2020).
- 813 5 Roche Diagnostics. *Elecsys Anti-SARS-CoV-2*, <<https://www.fda.gov/media/137605>>
814 (2020).
- 815 6 Schmidt, F. *et al.* Measuring SARS-CoV-2 neutralizing antibody activity using
816 pseudotyped and chimeric viruses. *J Exp Med* **217**, 284-218, doi:10.1084/jem.20201181
817 (2020).
- 818 7 Wajnberg, A. *et al.* Robust neutralizing antibodies to SARS-CoV-2 infection persist for
819 months. *Science (New York, N.Y.)*, eabd7728-7727, doi:10.1126/science.abd7728 (2020).
- 820 8 Seow, J. *et al.* Longitudinal observation and decline of neutralizing antibody responses in
821 the three months following SARS-CoV-2 infection in humans. *Nat Microbiol*, 1-17,
822 doi:10.1038/s41564-020-00813-8 (2020).
- 823 9 Brouwer, P. J. M. *et al.* Potent neutralizing antibodies from COVID-19 patients define
824 multiple targets of vulnerability. *Science (New York, N.Y.)* **369**, 643-650,
825 doi:10.1126/science.abc5902 (2020).
- 826 10 Cao, Y. *et al.* Potent Neutralizing Antibodies against SARS-CoV-2 Identified by High-
827 Throughput Single-Cell Sequencing of Convalescent Patients' B Cells. *Cell* **182**, 73-84
828 e16, doi:10.1016/j.cell.2020.05.025 (2020).
- 829 11 Ju, B. *et al.* Human neutralizing antibodies elicited by SARS-CoV-2 infection. *Nature*
830 **584**, 115-119, doi:10.1038/s41586-020-2380-z (2020).
- 831 12 Kreer, C. *et al.* Longitudinal Isolation of Potent Near-Germline SARS-CoV-2-
832 Neutralizing Antibodies from COVID-19 Patients. *Cell* **182**, 843-854 e812,
833 doi:10.1016/j.cell.2020.06.044 (2020).
- 834 13 Seydoux, E. *et al.* Analysis of a SARS-CoV-2-Infected Individual Reveals Development
835 of Potent Neutralizing Antibodies with Limited Somatic Mutation. *Immunity* **53**, 98-105
836 e105, doi:10.1016/j.immuni.2020.06.001 (2020).
- 837 14 Yuan, M. *et al.* Structural basis of a shared antibody response to SARS-CoV-2. *Science*
838 *(New York, N.Y.)* **369**, 1119-1123, doi:10.1126/science.abd2321 (2020).
- 839 15 Weisblum, Y. *et al.* Escape from neutralizing antibodies by SARS-CoV-2 spike protein
840 variants. *Elife* **9**, doi:10.7554/eLife.61312 (2020).
- 841 16 Barnes, C. O. *et al.* SARS-CoV-2 neutralizing antibody structures inform therapeutic
842 strategies. *Nature*, 1-25, doi:10.1038/s41586-020-2852-1 (2020).
- 843 17 Tortorici, M. A. *et al.* Ultrapotent human antibodies protect against SARS-CoV-2
844 challenge via multiple mechanisms. *Science (New York, N.Y.)* **4**, eabe3354-3316,
845 doi:10.1126/science.abe3354 (2020).

- 846 18 Baum, A. *et al.* Antibody cocktail to SARS-CoV-2 spike protein prevents rapid
847 mutational escape seen with individual antibodies. *Science (New York, N.Y.)* **369**, 1014-
848 1018, doi:10.1126/science.abd0831 (2020).
- 849 19 Li, Q. *et al.* The Impact of Mutations in SARS-CoV-2 Spike on Viral Infectivity and
850 Antigenicity. *Cell* **182**, 1284-1294 e1289, doi:10.1016/j.cell.2020.07.012 (2020).
- 851 20 Lamers, M. M. *et al.* SARS-CoV-2 productively infects human gut enterocytes. *Science*
852 (*New York, N.Y.*) **369**, 50-54, doi:10.1126/science.abc1669 (2020).
- 853 21 Livanos, A. E. *et al.* Gastrointestinal involvement attenuates COVID-19 severity and
854 mortality. *medRxiv*, 1-52, doi:10.1101/2020.09.07.20187666 (2020).
- 855 22 Qian, Q. *et al.* Direct evidence of active SARS-CoV-2 replication in the intestine. *Clin*
856 *Infect Dis*, 1-6, doi:10.1093/cid/ciaa925 (2020).
- 857 23 Han, Y. *et al.* Identification of SARS-CoV-2 Inhibitors using Lung and Colonic
858 Organoids. *Nature*, doi:10.1038/s41586-020-2901-9 (2020).
- 859 24 Morone, G. *et al.* Incidence and Persistence of Viral Shedding in COVID-19 Post-acute
860 Patients With Negativized Pharyngeal Swab: A Systematic Review. *Front Med*
861 (*Lausanne*) **7**, 562, doi:10.3389/fmed.2020.00562 (2020).
- 862 25 Park, S. K. *et al.* Detection of SARS-CoV-2 in Fecal Samples From Patients With
863 Asymptomatic and Mild COVID-19 in Korea. *Clin Gastroenterol Hepatol*, 1-11,
864 doi:10.1016/j.cgh.2020.06.005 (2020).
- 865 26 Wolfel, R. *et al.* Virological assessment of hospitalized patients with COVID-2019.
866 *Nature* **581**, 465-469, doi:10.1038/s41586-020-2196-x (2020).
- 867 27 Beaudoin-Bussieres, G. *et al.* Decline of Humoral Responses against SARS-CoV-2 Spike
868 in Convalescent Individuals. *mBio* **11**, 398-397, doi:10.1128/mBio.02590-20 (2020).
- 869 28 Crawford, K. H. D. *et al.* Dynamics of neutralizing antibody titers in the months after
870 SARS-CoV-2 infection. *J Infect Dis*, 1-15, doi:10.1093/infdis/jiaa618 (2020).
- 871 29 Iyer, A. S. *et al.* Persistence and decay of human antibody responses to the receptor
872 binding domain of SARS-CoV-2 spike protein in COVID-19 patients. *Sci Immunol* **5**,
873 eabe0367-0313, doi:10.1126/sciimmunol.abe0367 (2020).
- 874 30 Wang, K. *et al.* Longitudinal dynamics of the neutralizing antibody response to SARS-
875 CoV-2 infection. *Clin Infect Dis* **579**, 270-279, doi:10.1093/cid/ciaa1143 (2020).
- 876 31 Muecksch, F. *et al.* Longitudinal analysis of serology and neutralizing antibody levels in
877 COVID19 convalescents. *The Journal of Infectious Diseases*, doi:10.1093/infdis/jiaa659
878 (2020).
- 879 32 Schafer, A. *et al.* Antibody potency, effector function and combinations in protection
880 from SARS-CoV-2 infection in vivo. *bioRxiv* **182**, 828-826,
881 doi:10.1101/2020.09.15.298067 (2020).
- 882 33 Ripperger, T. J. *et al.* Orthogonal SARS-CoV-2 Serological Assays Enable Surveillance
883 of Low Prevalence Communities and Reveal Durable Humoral Immunity. *Immunity*, 1-
884 49, doi:10.1016/j.immuni.2020.10.004 (2020).
- 885 34 Liu, L. *et al.* Potent neutralizing antibodies against multiple epitopes on SARS-CoV-2
886 spike. *Nature* **584**, 450-456, doi:10.1038/s41586-020-2571-7 (2020).
- 887 35 Zost, S. J. *et al.* Potently neutralizing and protective human antibodies against SARS-
888 CoV-2. *Nature* **584**, 443-449, doi:10.1038/s41586-020-2548-6 (2020).
- 889 36 Nielsen, S. C. A. *et al.* Human B Cell Clonal Expansion and Convergent Antibody
890 Responses to SARS-CoV-2. *Cell host & microbe* **28**, 516-525 e515,
891 doi:10.1016/j.chom.2020.09.002 (2020).

- 892 37 Kaneko, N. *et al.* Loss of Bcl-6-Expressing T Follicular Helper Cells and Germinal
893 Centers in COVID-19. *Cell* **183**, 143-157 e113, doi:10.1016/j.cell.2020.08.025 (2020).
- 894 38 Victora, G. D. & Nussenzweig, M. C. Germinal centers. *Annu Rev Immunol* **30**, 429-457,
895 doi:10.1146/annurev-immunol-020711-075032 (2012).
- 896 39 Mahler, D. A. & Wells, C. K. Evaluation of clinical methods for rating dyspnea. *Chest*
897 **93**, 580-586, doi:10.1378/chest.93.3.580 (1988).
- 898 40 Pujadas, E. *et al.* SARS-CoV-2 viral load predicts COVID-19 mortality. *The Lancet.*
899 *Respiratory medicine* **8**, e70, doi:10.1016/S2213-2600(20)30354-4 (2020).
- 900 41 Chomczynski, P. & Sacchi, N. Single-step method of RNA isolation by acid guanidinium
901 thiocyanate-phenol-chloroform extraction. *Analytical biochemistry* **162**, 156-159,
902 doi:10.1006/abio.1987.9999 (1987).
- 903 42 DeAngelis, M. M., Wang, D. G. & Hawkins, T. L. Solid-phase reversible immobilization
904 for the isolation of PCR products. *Nucleic Acids Res* **23**, 4742-4743,
905 doi:10.1093/nar/23.22.4742 (1995).
- 906 43 Grifoni, A. *et al.* Targets of T Cell Responses to SARS-CoV-2 Coronavirus in Humans
907 with COVID-19 Disease and Unexposed Individuals. *Cell* **181**, 1489-1501 e1415,
908 doi:10.1016/j.cell.2020.05.015 (2020).
- 909 44 Amanat, F. *et al.* A serological assay to detect SARS-CoV-2 seroconversion in humans.
910 *Nat Med* **26**, 1033-1036, doi:10.1038/s41591-020-0913-5 (2020).
- 911 45 Barnes, C. O. *et al.* Structures of Human Antibodies Bound to SARS-CoV-2 Spike
912 Reveal Common Epitopes and Recurrent Features of Antibodies. *Cell* **182**, 828-842 e816,
913 doi:10.1016/j.cell.2020.06.025 (2020).
- 914 46 Schmidt, F. *et al.* Measuring SARS-CoV-2 neutralizing antibody activity using
915 pseudotyped and chimeric viruses. *J Exp Med* **217**, doi:10.1084/jem.20201181 (2020).
- 916 47 Weisblum, Y. *et al.* Escape from neutralizing antibodies by SARS-CoV-2 spike protein
917 variants. *bioRxiv* **17**, 1055-1042, doi:10.1101/2020.07.21.214759 (2020).
- 918 48 Gupta, N. T. *et al.* Change-O: a toolkit for analyzing large-scale B cell immunoglobulin
919 repertoire sequencing data. *Bioinformatics (Oxford, England)* **31**, 3356-3358,
920 doi:10.1093/bioinformatics/btv359 (2015).
- 921 49 Soto, C. *et al.* High frequency of shared clonotypes in human B cell receptor repertoires.
922 *Nature* **566**, 398-402, doi:10.1038/s41586-019-0934-8 (2019).
- 923 50 Guo, Y., Chen, K., Kwong, P. D., Shapiro, L. & Sheng, Z. cAb-Rep: A Database of
924 Curated Antibody Repertoires for Exploring Antibody Diversity and Predicting Antibody
925 Prevalence. *Front Immunol* **10**, 2365, doi:10.3389/fimmu.2019.02365 (2019).
- 926 51 Kyte, J. & Doolittle, R. F. A simple method for displaying the hydropathic character of a
927 protein. *J Mol Biol* **157**, 105-132, doi:10.1016/0022-2836(82)90515-0 (1982).
- 928 52 Guy, H. R. Amino acid side-chain partition energies and distribution of residues in
929 soluble proteins. *Biophysical journal* **47**, 61-70, doi:10.1016/S0006-3495(85)83877-7
930 (1985).
- 931 53 DeWitt, W. S. *et al.* A Public Database of Memory and Naive B-Cell Receptor
932 Sequences. *PLoS One* **11**, e0160853, doi:10.1371/journal.pone.0160853 (2016).
- 933 54 Spiegel, M. *et al.* Inhibition of Beta interferon induction by severe acute respiratory
934 syndrome coronavirus suggests a two-step model for activation of interferon regulatory
935 factor 3. *J Virol* **79**, 2079-2086, doi:10.1128/JVI.79.4.2079-2086.2005 (2005).
- 936 55 Mastronarde, D. N. Automated electron microscope tomography using robust prediction
937 of specimen movements. *J Struct Biol* **152**, 36-51 (2005).

938 56 Mastronarde, D. N. & Held, S. R. Automated tilt series alignment and tomographic
939 reconstruction in IMOD. *J Struct Biol* **197**, 102-113, doi:10.1016/j.jsb.2016.07.011
940 (2017).

941 57 Mastronarde, D. N. Correction for non-perpendicularity of beam and tilt axis in
942 tomographic reconstructions with the IMOD package. *Journal of microscopy* **230**, 212-
943 217, doi:10.1111/j.1365-2818.2008.01977.x (2008).

944 58 Yao, H. *et al.* Molecular Architecture of the SARS-CoV-2 Virus. *Cell*,
945 doi:10.1016/j.cell.2020.09.018 (2020).

946 59 Ke, Z. *et al.* Structures and distributions of SARS-CoV-2 spike proteins on intact virions.
947 *Nature*, doi:10.1038/s41586-020-2665-2 (2020).

948 60 Klein, S. *et al.* SARS-CoV-2 structure and replication characterized by in situ cryo-
949 electron tomography. *bioRxiv*, doi:10.1101/2020.06.23.167064v2 (2020).

950 61 Turoňová, B. *et al.* In situ structural analysis of SARS-CoV-2 spike reveals flexibility
951 mediated by three hinges. *Science* **370**, 203-208, doi:10.1126/science.abd5223 (2020).
952

953